Sustainable Cities and Society 148 (2026) 107641

Contents lists available at ScienceDirect

Sustainable Cities and Society

journal homepage: www.elsevier.com/locate/scs

High-resolution mapping and analysing urban building carbon emissions in the whole life cycle: The case of Guangzhou

Tong Sun [a,b], Canjie Liu [a], Francesco Pittau [b], Lingling Wu [a], Yabo Zhao [a,*]

[a] School of Architecture and Urban Planning, Guangdong University of Technology, Guangzhou, 510090, China

[b] Department of Architecture, Built Environment and Construction Engineering (DABC), Politecnico di Milano, via Ponzio 31, 20133 Milan, Italy

ARTICLE INFO

Keywords:
Building carbon emissions
Whole life cycle
Spatial analysis
Guangzhou

ABSTRACT

Building carbon emissions significantly drive climate change, yet obtaining high-resolution macro-scale data reflecting spatial variations remains a challenge. This paper proposes a novel method for calculating urban-scale carbon emissions based on building stock and big data mining. By inferring building ages using Points-of-Interest (POI) and the K-Nearest Neighbours (KNN) algorithm, and determining building types through integration with building vector and land use, the study constructs a high-resolution building carbon emissions map. The findings as follows: (1) Guangzhou's total building carbon emissions reached 1.079 billion tons. Carbon emissions were predominantly concentrated in the operational phase (57.3%). Residential, industrial, and commercial structures contributed significantly. (2) The carbon emissions exhibited a spatial pattern characterized by high-value concentration in the central urban area and low-value dispersion in peripheral zones. (3) Buildings constructed between 2000 and 2004 exhibit the highest carbon emissions, with per-unit emissions gradually increasing over time. Carbon emission hotspots demonstrate a dynamic temporal migration pattern of "expanding outward from the centre". (4) The potential for building demolition and material recycling is projected to peak in the 2030s, occurring earlier in core urban areas than in peripheral new districts. (5) Spatial coupling between building carbon emissions and population distribution is stronger than with GDP. Central urban areas exhibit efficient aggregation, while peripheral new districts show inefficient decoupling. This study provides quantitative evidence and methodological references for predicting and regulating building carbon emissions at the urban scale.

1. Introduction

1.1. Background

Global building carbon emissions account for about 28%−38% of the total global energy consumption carbon emissions (United Nations Environment Programme, 2020), therefore, the building sector has enormous potential for carbon reduction. However, revealing the high-resolution spatial distribution of building carbon emissions at the macro scale remains an urgent challenge to be solved. To this end, existing studies are reviewed, and a list of building carbon emission research is presented in Table 1. In previous studies, macro-scale building carbon emission research usually relies on socio-economic statistical data (Cavalliere et al., 2019) and remote sensing imagery (Zhang et al., 2025), and the data results represent the total building carbon emissions within a region (Zhang et al., 2022; Pu et al., 2022), but cannot reflect the spatial distribution of building carbon emissions within the region. This approach, which regards the region as the research and analysis unit, makes it difficult to carry out carbon reduction analysis within the region. Urban internal space is a complex and differentiated assemblage (Ito et al., 2024), and many studies have confirmed that urban spatial planning and spatial structure have significant impacts on carbon emissions (Yang et al., 2024; Christoforatos et al., 2025). Therefore, spatial research on carbon emissions is of great significance (Cook-Patton et al., 2020; Roncero-Tarazona et al., 2025). By analyzing the spatial distribution of carbon emissions, it is possible to deeply understand the characteristics and differences of carbon emissions in different areas, thereby identifying key regions and key industries of carbon emissions (Al-Qubati et al., 2024) and formulating targeted carbon reduction policies (Harris et al., 2021). Spatial research on carbon emissions can also provide scientific guidance for regional low-carbon development pathways (Abhijna et al., 2025),

* Corresponding author.
E-mail address: zhaoyabo3@163.com (Y. Zhao).

https://doi.org/10.1016/j.scs.2026.107641
Received 18 February 2026; Received in revised form 20 May 2026; Accepted 21 June 2026
Available online 22 June 2026

promote the coordinated development of carbon reduction and socio-economic development (Malekzadeh et al., 2025), and promote the realization of the United Nations Sustainable Development Goals (SDGs). High-resolution carbon emission maps can help scholars study the spatial distribution characteristics and influencing factors of carbon emissions within cities and help government managers reasonably allocate carbon reduction tasks and formulate feasible low-carbon development strategies (Cui et al., 2026).

The difficulty of establishing a high-resolution building carbon emission map at the macro scale lies in the fact that it is unrealistic to collect carbon emission inventories of each building from a macro perspective. In previous studies, Some scholars have attempted to estimate building carbon emissions using nighttime light and other remote sensing data, employing light brightness as an indicator of human activity intensity. Based on provincial or municipal-level carbon emission statistics, regression models—such as geographically weighted regression (GWR) and geographically and temporally weighted regression (GTWR) are constructed to downscale total regional carbon emissions to finer spatial units (Wang et al., 2024). However, constrained by the spatial resolution of remote sensing data, such approaches are unable to capture attribute differences such as building type and age. Moreover, remote sensing data only reflect emissions at a given static point in time, making it difficult to support refined management oriented toward the entire building life cycle. Unlike the indirect estimation logic of remote sensing, the assessment of the whole-life-cycle carbon emissions of buildings usually takes a single building as the research object (Hussien et al., 2023), and calculates its carbon emissions by collecting the material and construction inventories of the building in the whole life cycle stage (Felicioni et al., 2023), while the number of buildings within a province or city is too large to collect carbon emission data for each building.

However, with the gradual deepening of research, more and more scholars have begun to pay attention to certain characteristics shared by different buildings. By summarizing the parameters of different building types and analyzing their energy consumption, typical buildings of various types can be identified (Xu et al., 2024; Jungclaus et al., 2024; Nayak et al., 2023). The key to identifying typical buildings is to analyze the impact of building characteristics on energy consumption (Ma et al., 2025; Bampoulas et al., 2023). Once typical buildings are identified, the carbon emission inventory of buildings can be estimated according to their parameters (Chastas et al., 2018; Gauch et al., 2023), which is the key to realizing macro-scale research on the whole-life-cycle carbon emissions of buildings. However, due to information and technical limitations, there are still few studies extending the typical building carbon emission assessment model from single buildings to cities or larger-scale regions (Carnieletto et al., 2021), because of the lack of necessary macro urban building parameters corresponding to related typical buildings for carbon emission calculation.

Within this research stream, one line of work emphasizes fine-resolution spatial representation, combining Points-of-Interest (POI) data, road networks, and land-use information to capture intra-urban heterogeneity (Petrova-Antonova et al., 2025). A second group of

Table 1
Related studies on urban building carbon emissions in the whole life cycle.

Reference	Research scale	Building type	Research focus	Research method	Limitations
Wang et al., 2024	city-level / district-level / subdistrict-level	Residential, Commercial, Public	Comparing NTL data and regression models for multi-scale building carbon emission estimation	Nighttime light (NTL) imagery analysis; Geographically weighted regression (GWR)	**• Inability to account for building attributes and operational information • Limited fine-scale data availability**
Zhang et al., 2025	city-level / district-level	No differentiation of building types	Corrected NTL data to estimate carbon emissions at prefecture and county levels in China	Nighttime light (NTL) imagery analysis;Temporally Weighted Regression (GTWR)	**• Insufficient city- and county-level statistical data for error validation • Building types not differentiated**
Zhang et al., 2022	national level	Residential, Commercial	Scenario analysis of China's building stock, material demand, and embodied carbon dynamics	Stock dynamics model;Scenario analysis;Life Cycle Assessment (LCA)	**• Lack of data on renovation material intensity • Evolution of different building structural types not considered**
Pu et al., 2022	national level	No differentiation of building types	Projecting China's building sector carbon emissions and assessing carbon peak and neutrality feasibility	BP neural network model; Scenario analysis	**• Inter-provincial differences not considered • Inability to capture intra-regional variations • Reliance on historical trends**
Christoforatos et al., 2025	city-level	Residential	A dual functional unit method integrating residential density into building LCA	Life Cycle Assessment, (LCA) ; TOPSIS	**• Operational-stage impacts not included • Data on certain impact categories missing**
Felicioni et al., 2023	building level	No differentiation of building types	Life cycle environmental impact of a high-rise residential building in Denmark	Life Cycle Assessment, (LCA); Building Information Modeling (BIM)	**• Detailed structural calculations not performed • Structural effects of materials simplified • Reliance on a single case and a specific database**
Carnieletto et al., 2021	city-level / national level	Residential, Office	46 archetype building models for Italy's E climatic zone	Urban building energy model (UBEM);Building stock modelling	**• Geographical coverage concentrated in a single climate zone • Limited building typologies**
Fivet et al., 2024	city-level / building level	Residential, Office, Educational, Industrial & Retail	Spatiotemporal reconstruction of structural material use and embodied carbon in Geneva's buildings	Building stock modelling; Interpolation method; Life Cycle Assessment, (LCA)	**• Historical changes in carbon emission factors not incorporated • Insufficient data on building renovation and demolition**

studies adopts grid-based aggregation approaches, using population density or mobility data to improve the accuracy of large-scale urban carbon inventories, typically at the kilometer scale (Cai et al., 2021; Gao et al., 2023). In parallel, life-cycle-based frameworks have been increasingly applied to urban building stocks to account for both operational and embodied emissions in spatially explicit forms (Fivet et al., 2024).

1.2. Research gaps

As shown in Table 1, previous studies have advanced the estimation of building-related carbon emissions from different perspectives, including nighttime-light-based spatial downscaling, national or regional building-sector emission forecasting, single-building life-cycle assessment, urban building energy modelling, and building material stock analysis. Nevertheless, these studies still show several limitations when applied to high-resolution, whole-life-cycle building carbon emission assessment at the urban scale.

However, there are still several significant shortcomings in existing studies: (1) The research on building whole-life-cycle carbon emissions is still insufficient. Most studies focus only on energy consumption and carbon emissions during the operation stage, ignoring the carbon emissions in construction, maintenance, and demolition stages, leading to systematic bias in the estimation of total carbon emissions. (2) Key building information is missing, such as building age, structural type, and use function, which are simplified in most urban-scale studies. Most research adopts spatial proxy variables (such as POI and geographic distribution) to indirectly estimate carbon emissions, affecting the accuracy of typical building identification and inventory compilation. (3) Many studies mainly focus on overall urban-scale carbon emissions but do not specifically refine to the building carbon emission level, making it difficult to reveal carbon emission differences at the micro-scale such as different building types and structures. (4) Research on the coupling relationship between building carbon emissions and socio-economic factors such as urban population density and GDP is still limited. Most studies focus on total carbon emissions or industrial classification, lacking spatial heterogeneity analysis, making it difficult to support differentiated carbon reduction strategies.

1.3. Contributions of this study

This study proposes a method integrating multi-source data to supplement key information such as building age and type, and on this basis, conducts whole-life-cycle building carbon emission measurement and analysis at the urban scale. Taking Guangzhou as a case, a 100 m resolution building carbon emission map was constructed, thereby revealing significant spatial differences and temporal characteristics within the city. On this basis, the marginal contributions of this study are as follows:

(1) refined the city-scale accounting method for whole-life-cycle building carbon emissions, and analyzed the total amount, composition, and temporal evolution (historical-current-future) of Guangzhou's building carbon emissions;
(2) further disaggregated the carbon emission differences across different building ages and types within various administrative districts;
(3) constructed a high-resolution spatial distribution pattern of high-emission hotspot areas at 100-meter resolution; and revealed the spatial coupling relationship between building carbon emissions, population, and GDP, and projected the future potential of building demolition and material recycling.

The research results not only reveal the spatiotemporal characteristics of building carbon emissions in Guangzhou but also provide a scientific basis for differentiated carbon reduction policies at the urban level.

2. Data and methods

2.1. Study area

Guangzhou is located in the south of China and is an important economic centre and transportation hub in southern China (Fig. 1). Guangzhou has a total area of 7434.4 km^2, with a resident population of 18,734,100 and a GDP of 3.203 trillion yuan in 2025. Guangzhou is considered to be one of the fastest-growing cities in the world today, and its rapid urbanization has led to an accelerated depletion of natural resources and exacerbated energy consumption (Zhou et al., 2018). Studying its building carbon emissions and emission reduction strategies is of positive significance for advancing building carbon emission reduction in southern China. In addition, Guangzhou also has a rich architectural culture and building types, which are pivotal to the study of building carbon emission reduction technologies, strategies, and practices. Therefore, Guangzhou is a suitable case for building carbon emission reduction research with typicality, representativeness, and urgency.

2.2. Data

The building base vector data of Guangzhou comes from Baidu Company (https://www.baidu.com/), which has a total of 366,787 buildings. It contains three kinds of information: basic geographic location, geometry and floor height of each building. Due to the lack of original data, the dataset does not include all areas of Guangzhou but includes densely populated areas in and around the city centre of Guangzhou (Fig. 1). The total area of the covered area is 394km^2, which contains the vast majority of Guangzhou's population, economy, and the core built-up area. Thus, it is sufficient to meet our research needs.

Building vector data refers to the recording of a building's geographical information using vector data formats, including its location, geometric shape, area and height. The foundational vector data for Guangzhou's buildings utilised in this research originates from Baidu (https://www.baidu.com/). After importing the data into GIS software for processing and analysis, including operations such as removing duplicate records and correcting outliers, a total of 366,787 buildings were identified.

To verify the reliability of the Baidu building vector dataset used in this study, the total floor area of each district in 2020 was estimated based on the *Guangzhou Statistical Yearbook (2020)* using two official indicators: the permanent resident population and the per capita floor area. The results were then compared with the Baidu-derived floor area data. Table 2 presents the total floor area of each district from both sources and their relative errors. The overall discrepancy between the Baidu dataset and the official statistics was only 5.8%, demonstrating that the dataset provides an accurate and representative reflection of Guangzhou's overall building stock.

For Guangzhou's four central urban districts (Yuexiu, Haizhu, Liwan, and Tianhe) along with the relatively central Baiyun and Huangpu districts, dataset discrepancies remained below 10%. Huadu and Panyu exhibited comparatively larger errors of 17.4% and 25.3% respectively. Considering the differing statistical methodologies of the two data sources, the error margins for these eight major administrative districts fall within an acceptable range. Nansha, Conghua, and Zengcheng, situated on the periphery of Guangzhou, were excluded from the analysis due to data gaps and significant discrepancies between their Baidu dataset and official records. Consequently, the analysis represents Guangzhou based on the remaining eight administrative districts (Fig. 1).

Since the basic building data does not contain building type and age information, this study derives these two basic information in the following way:

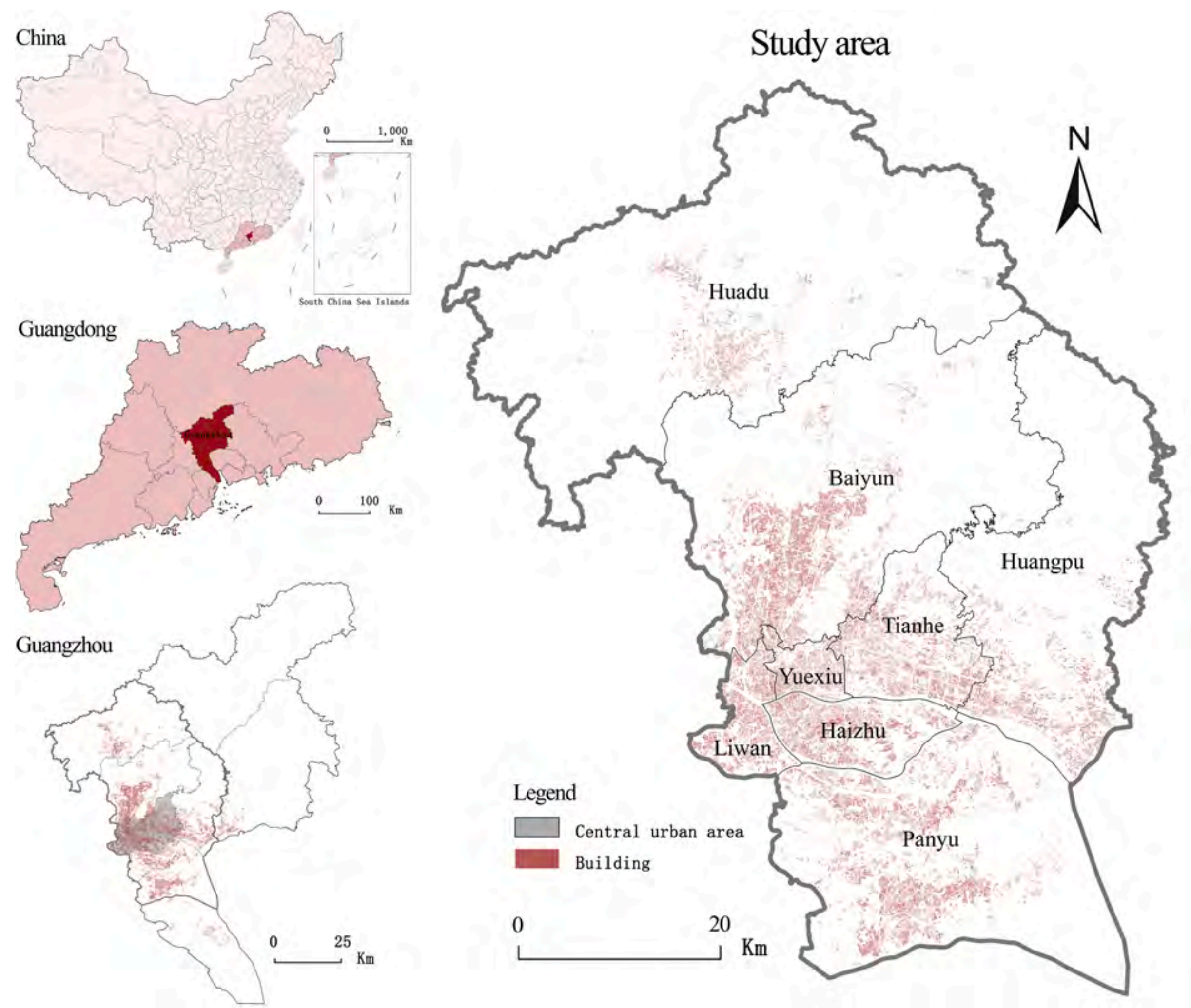

Fig. 1. Study area.

Table 2
Building dataset coverage by zoning district.

District	Number of Buildings	Building Area (10,000 m^2)		Error (%)
		Baidu Dataset	Official Statistical Yearbook	
Yuexiu	18,005	3936.4	3587.7	9.7%
Haizhu	53,102	6767.8	6298.3	7.5%
Liwan	20,756	4011.2	4297.2	6.7%
Tianhe	45,695	7322.7	7790.7	6.0%
Baiyun	73,516	14,262.4	13,010.2	9.6%
Huangpu	40,362	4758.4	4392.7	8.3%
Huadu	13,198	4717.6	5713.8	17.4%
Panyu	84,984	11,589.2	9249.9	25.3%
Guangzhou	366,787	61,094.0	64,860.2	5.8%

Derivation of building age: Referring to Mao et al.'s study (Mao et al., 2020), a big data analytics approach was used to assign POI information to each building by matching the nearest building centroids with Baidu's residential/commercial POI data. Web crawlers were used to collect from four of the largest real estate agency websites in China (Lianjia, Beike, Fangtianxia and Anjuke) to get the building construction date and geographic location information. Using the collected location information, we searched for the nearest POIs and finally obtained the age information of 86.4% of the buildings in the study area.

For the remaining buildings without age records, the K-Nearest Neighbours (KNN) algorithm was employed for age inference. The KNN method is based on the assumption that buildings located in close spatial proximity tend to share similar construction periods because of common urban development processes. In this study, building centroid coordinates were used as the input features, and Euclidean distance was adopted to identify neighbouring samples.

To quantitatively validate this inference framework and determine the optimal K value, we conducted a 10-fold cross-validation using the age-labelled building samples. Specifically, the labelled samples were randomly divided into ten subsets; in each round, nine subsets were used for training and the remaining one subset was used for validation, and this process was repeated ten times. To avoid subjective parameter selection, a range of candidate K values was tested, and the average validation accuracy across the ten folds was compared. The results showed that the best-performing parameter was K = 3, under which the model achieved an overall validation accuracy of 91.2%. This result exceeds the minimum accuracy threshold of 85% proposed by the USGS (Anderson et al., 1976). The optimized KNN model was then applied to infer the construction years of the remaining unlabeled buildings.

Derivation of building types: Based on the 30m*30 m land use data released by Tsinghua University (Gong et al., 2020), the spatial overlay analysis of the building vector data was performed to assign a building type to each building.

Eleven building-related land use types were selected from the publicly available land use data of Tsinghua University. As the vast majority of the research data and the building energy consumption coefficients summarized in the literature grouped some of the building types that are different in the land use classification into one category. For example, cultural, sports and recreational land use and educational land use in the land use types are united into cultural and educational buildings, etc. Therefore, some of the land use types were merged and finally, seven building archetypes were defined, namely: residential, factory, office, commercial building, education and culture, medical building and other building types. Among them, the other building types mainly include buildings classified by land use types such as airport facilities, transport stations and parks and greenspaces.

Based on the derivation methodology, the results of the derivation of Guangzhou's architectural periods and building types, along with their quantitative distributions, are presented in Tables 3 and 4 respectively.

2.3. Methodology

2.3.1. Defining the system boundary

This study proposes an improved method for estimating urban building energy consumption and carbon emissions based on building stock and establishes a building energy consumption calculation model based on the whole life cycle process, The detailed technical route is illustrated in the Fig. 2. According to different research purposes and contents, previous studies have divided the building life cycle stages differently. In this section, some important concepts and scopes of the model are defined as follows:

On the basis of existing studies, the whole process of a building is divided into five processes: material production and preparation, transport of building materials, building construction, building operation, and building demolition (Huo et al., 2020; Ng et al., 2012). Therefore, the calculation of the whole life cycle carbon emissions of a building can be defined as:

$$BCE = ME + TE + CE + OE + DE \tag{1}$$

Where *BCE* is building carbon emission; *ME* is material production and preparation energy consumption; *TE* is material transport energy consumption; *CE* is building construction energy consumption; *OE* is building operation energy consumption; and *DE* is building demolition energy consumption. The unit for all energy types is CO_2e.

2.3.2. Intensity of construction material consumption

There are generally eight types of building materials commonly used in China, including steel, timber, cement, brick, gravel, asphalt, lime and glass (Cao et al., 2018). There are no industry codes or manuals that contain the intensity of building material consumption for different structural buildings. It is impractical to collect the bill of quantities associated with each building at the city scale (Oregi et al., 2018; Pereira & Ramos, 2018), therefore, this study used an aggregated approach to calculate the material consumption for each prototype in the building inventory, and a total of eight major building consumables that account for >90% of the total carbon emissions were considered (Yang et al., 2020). The intensity of building material consumption for each building type was summarized and generalized by researching a large number of literature and manuals (Cao et al., 2018; Heeren & Fishman, 2019; Huang et al., 2018; Chang et al., 2016; Z.Luo et al., 2019). A total of >1100 material lists were collected for the building samples. Containing all building prototypes defined in this study, these building samples were categorized into four age echelons (pre-1950, 1951–1980, 1981–2000 and 2001–2020). The material consumption intensity factors varied considerably depending on the age of construction and the type of use of the building. Table 5 lists the material consumption intensities of the eight common building materials summarized in this study.

Table 3
Number and proportion of building years in Guangzhou.

Building years	Number of buildings	Proportions
Pre-1980	8346	0.023
1980–1984	8771	0.024
1985–1989	15,548	0.042
1990–1994	40,191	0.109
1995–1999	83,300	0.227
2000–2004	133,989	0.365
2005–2009	34,914	0.095
2010–2014	22,883	0.063
2015–2020	18,845	0.052

Table 4
Description and number of building types in Guangzhou.

Type	Description	Number of buildings	Proportions
Residential	Residential land, houses and apartments.	129,401	0.353
Factory	Land and buildings used for manufacturing, warehousing, mining, etc.	104,190	0.284
Office	Buildings where people work, including office buildings, commercial offices in finance, internet technology, e-commerce, and media.	6975	0.019
Commercial	Houses and buildings used for commercial retail, restaurants, lodging and entertainment.	42,672	0.116
Education and Culture	Land for education and research, including campuses and research institutes; land for public sports training and cultural services, including fitness centres, libraries, museums, exhibition centres, etc.	40,757	0.111
Medical	Buildings for hospitals, disease prevention and emergency services.	8733	0.024
Others	Types of airport facilities, transit stations, and parklands.	34,059	0.093

Therefore, the material consumption per building can be calculated by the following equation:

$$MC = \Sigma_{i,j,t} MCI_{i,j,t} \times Q \tag{2}$$

Where *MC* is the material consumption; *MCI* is the material strength factor per square metre of the building; *Q* is the total area of a single building; *i* is the type of material; *j* is the type of building; and *t* is the age of the building.

2.3.3. Uncertainty analysis within the MCI group

To assess the robustness of the grouped-average MCI assignment, a sensitivity analysis was performed to construct alternative year-specific MCI trajectories within each broad age group. Instead of assuming a constant MCI value for all buildings within the same age interval, annual MCI values for each building type-material combination were represented by a continuous piecewise-linear function over 1951–2020, constrained by the literature-derived grouped MCI means and the observed building-area distribution by construction year. Based on this framework, two perturbed scenarios were generated in addition to the baseline grouped-average assignment: a minimum-deviation scenario, which remained as close as possible to the baseline path, and a maximum-deviation scenario, which represented the largest admissible departure from the baseline under the imposed constraints. The detailed parameterization, search ranges, hierarchical screening strategy, and treatment of unresolved combinations are provided in Support information 1.

These scenario-specific annual MCI values were then matched to individual buildings according to construction year and building type, and material stocks were recalculated by multiplying the corresponding MCI by building area. The resulting material stocks were further used to recalculate embodied carbon, allowing us to examine whether the main results were sensitive to possible within-group temporal variation in

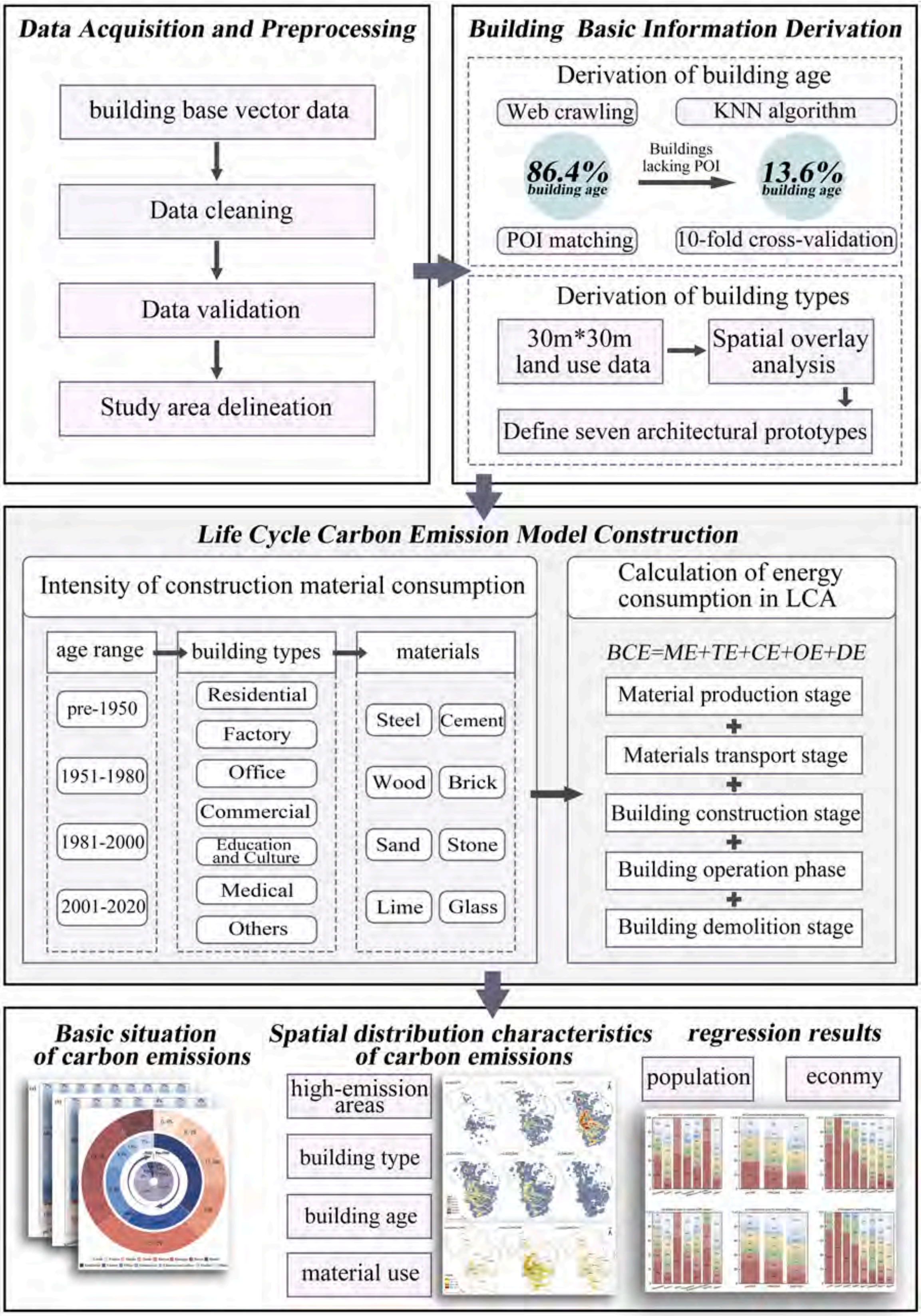

Fig. 2. Technical route of this study.

Table 5
Strength factor of construction materials (Kg/m^2).

Age range	Building type	Steel	Cement	Wood	Brick	Sand	Stone	Lime	Glass
2001–2020	Residential	56	199	18	330	541	321	57	2
	Factory	37	209	20	393	653	729	39	2
	Office	86	219	30	326	346	266	27	3
	Commercial	103	239	31	389	361	364	27	2
	Education and culture	66	214	21	279	340	329	33	3
	Medical	92	201	25	352	440	407	32	2
	Others	66	191	21	325	415	373	32	2
1981–2000	Residential	22	153	18	742	628	432	33	3
	Factory	59	98	25	289	322	286	22	2
	Office	44	181	21	632	656	488	30	4
	Commercial	53	202	21	637	720	515	31	4
	Education and culture	42	175	17	690	620	570	27	4
	Medical	46	160	21	838	572	337	38	3
	Others	43	158	23	741	608	434	37	3
1951–1980	Residential	18	68	39	641	273	195	20	1
	Factory	12	74	32	718	517	229	16	1
	Office	10	68	27	777	343	203	19	1
	Commercial	2	11	35	456	167	237	21	1
	Education and culture	9	54	25	802	363	219	25	1
	Medical	1	10	24	413	156	225	12	1
	Others	2	30	31	902	398	531	26	1
Pre-1950	Residential	12	88	77	635	277	380	14	2
	Factory	5	46	62	633	579	428	7	2
	Office	1	12	53	768	260	380	19	2
	Commercial	4	21	70	913	334	473	41	2
	Education and culture	5	16	51	708	299	415	19	2
	Medical	3	21	47	827	311	450	24	2
	Others	1	20	63	873	495	1054	17	2

MCI. If the baseline, minimum-deviation, and maximum-deviation scenarios produce similar results, the grouped-average MCI assignment can be regarded as sufficiently robust for the purpose of this study.

2.3.4. Calculation of energy consumption in LCA

2.3.4.1. Material production stage. The CO_2 in the production process of building materials can be calculated using the product of the amount of various building materials and the corresponding carbon emission factor. The carbon emission factors of various building materials are borrowed from several research results from China itself (Z.Luo et al., 2019; Dezhi et al., 2015; Zhang & Wang, 2016), and the specific factors are shown in Table 6, and the calculation formulas are as follows:

$$\mathrm{ME}=\Sigma_i \mathrm{MC_i} \times \mathrm{EF_i} \tag{3}$$

Where *ME* is the emission of CO_2 during the production of building materials; MC_i is the amount of *i* building material used in the building; EF_i is the carbon emission factor of *i* building material used in the building.

2.3.4.2. Building materials transport stage. The commonly used transport modes for building materials are railway, road, water transport, and air transport. According to a research report by the Guangdong Provincial Department of Transport (Lin et al., 2021), the transport mode of relevant building materials in Guangdong Province is dominated by road diesel vehicles, and new energy vehicles are gradually rising, but the current proportion is still small, at the same time, the transport within Guangdong Province occupies an absolute advantage compared to the transport outside the province, with a proportion as high as 95.5%. Considering the principle of proximity of building materials transport, this paper approximates that the radius of building materials transport is the same, therefore, referring to the average transport distance of building materials in the statistics of the literature (Geng et al., 2022), by default, all building materials are transported by diesel trucks by road, and the average transport distance of the main building materials is shown in Table 7. Dividing it by the fuel efficiency to get the fuel consumption per unit of transport, and then according to the diesel fuel carbon emission factor of 0.196 $kgCO_2e/t\cdot km$ (Luo, 2016), the CO_2 emission factor for the building materials transport phase was calculated.

$$\mathrm{TE}=\Sigma_i \mathrm{MC_i} \times \mathrm{EF_{l,i}} \times \mathrm{D_i} \tag{4}$$

Where *TE* is the carbon dioxide emission during the transport of building materials; MC_i is the quantity of *i* building materials used in the building; $EF_{l,i}$ is the carbon emission factor transporting one unit of cargo per kilometre by diesel vehicle; D_i is the transport distance of *i* building materials used in the building.

2.3.4.3. Building construction stage. The process of building construction mainly includes civil engineering works, water supply and drainage works, electrical works, HVAC works and decoration works. The main sources of carbon emissions in the construction stage are electricity consumption for construction and oil consumption for construction, including direct carbon emissions (e.g. diesel used for transporting earth and pumping concrete, carbon emissions caused by diesel combustion, etc.) and indirect carbon emissions (e.g. carbon emissions caused by electricity consumption for construction, etc.). (Luo et al., 2016) constructed a calculation model of carbon dioxide emissions during the building construction stage and concluded that the higher the building height, the greater the carbon emissions per unit area. The study was conducted separately for three kinds of buildings with different heights, which is of great reference value to this paper. Through collation, the

Table 6
Carbon emission factors at the material production stage ($kgCO_2e/kg$).

Building material	Steel	Cement	Wood	Brick	Sand	Stone	Lime	Glass
Carbon emission factors	2.31	0.977	0.257	0.155	0.003	0.003	1.99	1.19

Table 7
Carbon emission factors for the transportation phase of building materials.

Building material	Steel	Cement	Wood	Brick	Sand	Stone	Lime	Glass
Average transportation distance (km)	125	28	35	39	13	40	30	80

carbon emission per unit area of each sub-project in the construction process is shown in Table 8. The formula is as follows:

$$CE=\Sigma_{i,j}EF_{i,j} \times Q \tag{5}$$

Where *CE* is the emission of CO_2 during building construction, $EF_{i,j}$ is the value of the carbon emission factor for *j* projects of building type *i*, and *Q* is the total area of the building itself.

2.3.4.4. Building operation phase. The operation and use phase is the longest and largest carbon emission phase in the whole life cycle of a building, and it has a significant impact on the evaluation of carbon emissions. The operational carbon emissions and calculation methods of different building types vary greatly. In this section, we discuss residential and public buildings separately. Since the energy consumption of industrial buildings is included in the “industrial” energy consumption, it is not considered in this paper. Instead, we consider the energy consumption of industrial buildings for non-industrial activities, i.e. human activities, and replace this with the average energy intensity of public buildings.

2.3.4.4.1. Building lifespan. According to the findings of Cao et al. (Cao et al., 2019), the building lifespan in South China is approximately 38 years; however, the study indicates that in rapidly developing areas such as Shenzhen, the building lifespan is about 24 years. Another study by Cai et al. (Cai et al., 2025). reports that the building lifespan in Guangdong Province is approximately 45.3 years. Since 2000, building lifespans in China have exhibited an increasing trend. Most studies commonly assume a building lifespan in China within the range of 35–50 years (Zhu et al., 2022; Liu et al., 2023; Pei et al., 2024). Given the specific development context of Guangzhou and with reference to the aforementioned studies, this paper adopts a 35-year lifespan as the baseline assumption. Furthermore, service lives of 25, 50, and 70 years are introduced for multi-scenario analysis.

2.3.4.4.2. Residential. According to a large-scale statistical survey conducted by the Ministry of Housing and Urban-Rural Development of China on the energy consumption of civil buildings in several cities (Ding et al., 2009), residential energy consumption is dominated by electricity and natural gas, accounting for 71% and 20.28% of the total energy consumption, respectively. The energy consumption per unit area of residential buildings in the hot summer and warm winter region (Guangzhou belongs to the hot summer and warm winter region) is 57.23kWh/(m^2·a), and the electricity factor in the South is 0.527kg/kWh. Previous studies have largely indicated that residential buildings constructed before 2000, between 2000 and 2010, and after 2010 exhibit notable differences in the external wall heat transfer coefficient, window heat transfer coefficient, solar heat gain coefficient, and cooling energy efficiency ratio, with newer buildings generally demonstrating superior building envelope performance and cooling system efficiency. To reflect variations in operational energy consumption among residential buildings of different construction periods, this study refers to prior research (Yigit et al., 2025) and adopts residential buildings from the 2000–2010 period as the baseline, assigning an adjustment factor of 1.10 to pre-2000 buildings and 0.90 to post-2010 buildings.Therefore, the building operation energy consumption of residential buildings is calculated by the formula:

$$OE_r=EF_r \times Q \times EF_e \times n \tag{6}$$

Where OE_r is the CO_2 emission during the operation of the residence, EF_r is the energy consumption per unit area of the residence, EF_e is the value of the Southern Electricity Factor, *Q* is the total area of the building itself, and *n* is the time of operation of the building.

2.3.4.4.3. Public and industrial buildings. Public buildings mainly include commercial, educational cultural, medical etc. Energy consumption is mainly electricity energy consumption. Based on the research report of the Guangdong Academy of Building Science on monitoring the electricity consumption of public buildings in the Pearl River Delta region (Zhou, 2022), the electricity consumption of the main types of public buildings in Guangzhou required for this paper is collated and shown in Table 9. To further reflect the impact of building scale and construction characteristics on the energy use intensity of public buildings during the operational phase, this study introduces an adjustment factor based on the baseline operational energy consumption values for buildings in the Guangdong region, with reference to the findings of a study on the energy use intensity of public buildings in the Hot Summer and Warm Winter zone (Deng, 2020). That study surveyed the annual electricity consumption and basic building information of 317 office buildings in the Hot Summer and Warm Winter zone and analyzed the effects of factors such as building age and floor area on the energy consumption index per unit floor area.

For the calculation of the adjustment coefficients, a proportional normalization method is adopted. Specifically, for the two factors that most significantly influence energy consumption, construction period and floor area, the mean energy consumption per unit floor area of all subgroups under each variable is taken as the baseline value. The adjustment coefficient for each subgroup is then obtained by dividing its energy consumption per unit floor area by the corresponding baseline value:

$$F_j = E_j/\overline{E} \tag{7}$$

Where F_j is the operational energy consumption adjustment factor for subgroup *j*, E_j is the energy consumption per unit floor area of that subgroup, and $\bar{E}$ is the average energy consumption per unit floor area across all subgroups under the same categorical variable. Based on this method, the adjustment factors for construction period and floor area for public buildings were derived, as presented in Table 10.

The final energy consumption per unit floor area of public buildings during the operational phase is calculated as follows:

$$E_{public}=E_{0,public} \times F_{year} \times F_{area} \tag{8}$$

Where E_{public} is the adjusted operational energy consumption per unit floor area of public buildings, $E_{0,public}$ is the baseline value of operational energy consumption for public buildings in the Guangdong region, F_{year} is the construction period adjustment factor, and F_{area} is the floor area adjustment factor.

The formula is as follows:

$$OE=EF_i \times Q \times EF_e \tag{9}$$

Table 8
Carbon emission factors for sub-projects during the construction phase of the project ($kgCO_2e/m^2$).

Itemized project	Under 24m	24~100m	Over 100m
Civil engineering	215.93	239.25	280.51
Water supply and drainage engineering	2.02	2.59	7.45
Electrical engineering	2.22	3.45	9.99
HVAC engineering	4.35	6.82	21.47
Decoration works	28.93	30.15	36.62
Building Construction	18.54	24.3	45.66
All	271.99	306.56	401.7

Table 9
Energy consumption per unit area during the operational phase of a building (kWh/(m^2·a)).

Type	Residential	Factory	Office	Commercial	Education and Culture	Medical	Others
Energy consumption per unit area	57.23	55.15	51.65	128.94	24.66	95.43	27.38

Table 10
Table of adjustment factors.

Construction period	Adjustment factor	Floor area	Adjustment factor	Residential	Adjustment factor
Before 2000	0.91	<10,000 m^2	0.9	Before 2000	1.15
2000–2010	0.96	10,000–20,000 m^2	0.9	2000–2010	1
After 2010	1.17	20,000–30,000 m^2	0.9	After 2010	0.85
		30,000–40,000 m^2	1		
		40,000–50,000 m^2	1		
		50,000–60,000 m^2	1.2		
		>60,000 m^2	1.1		

Where *OE* is the amount of CO_2 emitted during the operation of the building, EF_i is the energy consumption per unit area of the building in category *i*, EF_e is the value of the Southern Electricity Factor, and *Q* is the total area of the building itself.

2.3.4.5. Building demolition stage. The building demolition stage was divided into three processes: demolition waste generation, waste transportation, and final disposal. Considering the limited availability of city-scale demolition inventory data, this study estimated demolition-stage carbon emissions based on material stock and process-based emission factors. The energy consumption of demolition machinery was mainly derived from a local field investigation of building demolition projects in Guangzhou (Liu et al., 2020), which provides representative parameters for machinery types, work efficiency, energy type, and energy consumption rates under the local construction and demolition context. The corresponding machinery-operation data are listed in Table 12.

In the waste generation process, demolition machinery is used to dismantle buildings, collect demolition waste, and conduct on-site sorting and handling. The carbon emissions from this process were calculated by multiplying the energy consumption of each type of machinery by the corresponding carbon emission factors for diesel-powered or electric equipment.

In the transportation process, demolition waste generated from each building was assumed to be transported by diesel trucks via road to the disposal facility. The transportation-related carbon emissions were calculated based on the mass of demolition waste, the average transport distance, and the corresponding diesel-truck emission factor.

In the final disposal process, this study adopted a conservative baseline assumption that all demolition waste is sent to landfill, without considering material recycling or avoided emissions from recycled material substitution. Therefore, the disposal emissions were estimated by multiplying the mass of landfilled waste materials by the corresponding landfill carbon emission factors. The landfill emission factors for different waste materials are shown in Table 11.

Table 11
Carbon emission factors for material landfilling.

Waste Materials	Carbon Emissions Factors of Chemical Reaction ($kgCO^2eq./t$)
Steel	454.8083
cement	8.7033
wood	5102.6140
brick	8.7033
sand	8.7033
stone	8.7033
lime	8.7033
glass	55.5330

Table 12
Energy consumption of machinery operation in the demolition phase.

Waste Materials	Work Efficiency	Energy Type	Energy Consumption Rate
Rockdrill	0.364608h/m^2	Electricity	15.7kwh/h
Hydraulic hammer	0.043801h/m^2	Diesel	18.9kg/h
Crawler bulldozer	0.025874h/m^2	Diesel	17.8kg/h
Crawler hydraulic rock crusher	0.138606h/m^2	Diesel	27.2kg/h
Electromagnetic separator	0.001707h/t	Electricity	11.0kwh/h
Conveyor belt	0.001707h/t	Electricity	15.0kwh/h
Vibration feeder	0.001913h/t	Electricity	13.0kwh/h

The carbon emissions from the building demolition stage were calculated as follows:

$$DE=\sum_j C_{mach,j}+\Sigma_i MC_i \times EF_{l,i} \times D_i+\sum_i(M_i \times f_i) \quad (10)$$

Where *DE* is the total CO_2 emissions from the building demolition process; $C_{mach,j}$ is the CO_2 emissions generated by machinery type j during demolition; MC_i is the mass of waste material type i involved in transportation; $EF_{l,i}$ is the carbon emission factor for transportation of waste material type i; D_i is the average transport distance from the site to the corresponding disposal facility; M_i is the mass of waste material type i sent to landfill; f_i is the carbon emission factor for landfilling.

3. Results

3.1. Basic situation and verification of carbon emissions

The total carbon emissions from existing buildings in Guangzhou amount to 1.079 billion tonnes (Fig. 3). This figure underscores the critical role of Guangzhou's buildings in addressing climate change challenges. Among these, carbon emissions from the operational phase of buildings accounted for the largest share at 57.3% of the total. In contrast, emissions from material production, construction, transportation, and demolition phases were relatively lower, representing 24.2%, 15.9%, 0.6%, and 1.8% of the total respectively. These findings are consistent with most domestic and international research outcomes (Zhang & Wang, 2016).

Significant disparities are observed among different building types in Guangzhou in both total carbon emissions and emission intensity per unit area. Residential buildings contribute the largest share of total emissions, reaching 425 million tonnes CO_2e, accounting for 39.4% of the total building-related emissions. In contrast, office and medical

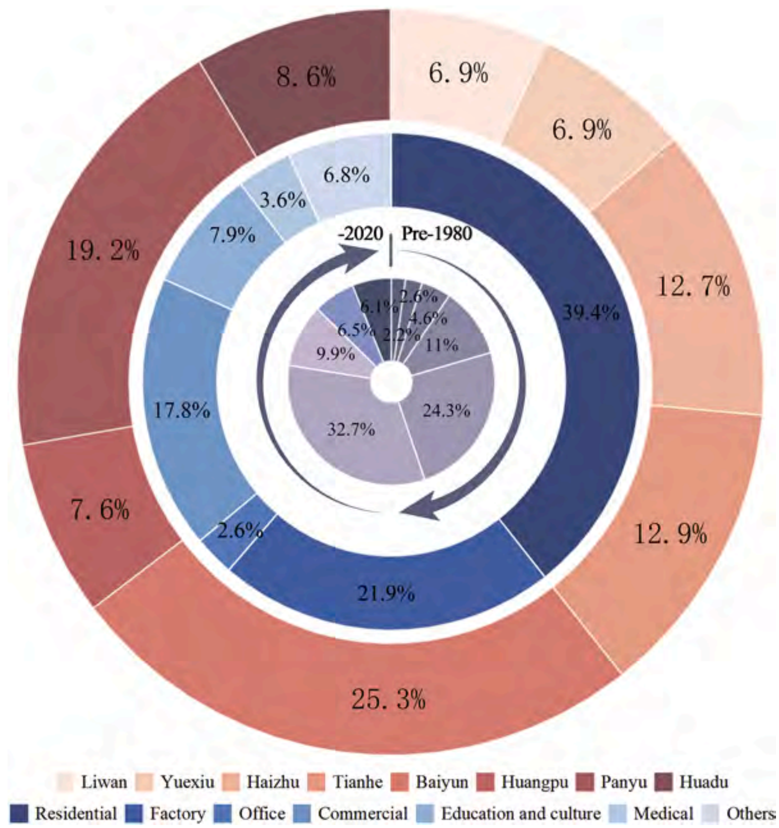

Fig. 3. Carbon emission share of buildings in Guangzhou.

buildings have the lowest proportions, representing only 2.6% and 3.6%, respectively (Fig. 4). The emission intensity per unit area of commercial and medical buildings is substantially higher than that of other types, amounting to 2894 $kgCO_2e/m^2$ and 2323 $kgCO_2e/m^2$, respectively, whereas "other" building types emit only 1214$kgCO_2e/m^2$, a difference of more than twofold (Table 13). Moreover, as shown in Fig. 4(b), the operation stage remains the dominant contributor to life-cycle carbon emissions across most building categories. For instance, operational emissions account for 71% of the total in commercial buildings and 65% in medical buildings. In contrast, educational and cultural buildings exhibit a more balanced pattern: operational emissions constitute only 24%, while embodied carbon from material production (39%) and construction (24%) together represent 63% of total life-cycle emissions, highlighting that their upfront carbon footprint should not be overlooked.

Marked spatial variations in building carbon emissions are also evident across Guangzhou's administrative districts (Fig. 3). Among them, Baiyun District records the highest total emissions, reaching 25 $MtCO_2e$ (25.3% of the city's total), followed by Panyu (19.2%) and Tianhe (12.9%). The lowest emissions occur in Yuexiu (6.9%) and Liwan

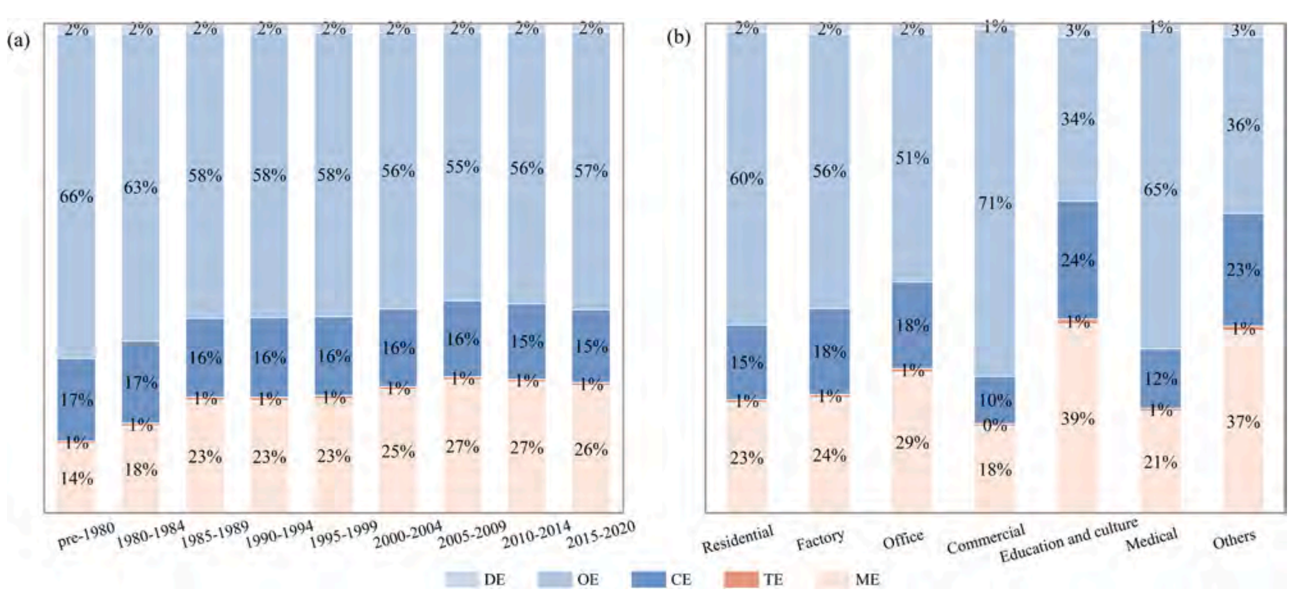

Fig. 4. Proportion of carbon emissions from the whole life cycle stage of a building.

Table 13
Carbon emission characteristics of different building types.

Building type	Total carbon emissions ($WtCO_2e$)	Percent	Carbon emissions ($kgCO_2e/m^2$)
Residential	42,485	39.4%	1872
Factory	23,641	21.9%	1574
Office	2838	2.6%	1614
Commercial	19,195	17.8%	2894
Education and culture	8509	7.9%	1165
Medical	3904	3.6%	2324
Others	7282	6.8%	1214

(6.9%) districts. From the perspective of emission density (Table 14), Yuexiu District exhibits the highest intensity at 205 tCO_2/km^2, followed by Haizhu (142 tCO_2/km^2) and Liwan (118 tCO_2/km^2). In contrast, Huadu shows the lowest emission density (9 tCO_2/km^2), and Huangpu also remains at a relatively low level (16tCO_2/km^2). Overall, these findings reveal pronounced spatial heterogeneity: the central urban districts, characterized by intensive land development, high building density, and strong emission clustering, display a distinct "high-density, high-carbon" pattern.

Substantial differences also exist across construction periods (Fig. 3; Table 15). Buildings constructed between 2000 and 2004 account for 32.73% of total emissions, followed by those built in 1995–1999 (24.3%). In contrast, buildings erected before 1980 contribute only 2.2%. Meanwhile, the carbon emission intensity per unit area has shown a consistent upward trend (Table 15). The life-cycle structure of emissions has also evolved markedly over time (Fig. 4(a)), shifting gradually from an "operation-dominated" to a "whole-cycle distributed" pattern. Before 1980, operational emissions accounted for as much as 66%, while emissions from material production and construction together contributed only 15%. Over time, the share of operational carbon emissions has gradually declined,while the combined proportion of material production and construction has risen to 28%, reflecting the growing importance of embodied carbon in recent decades.

3.2. Spatial distribution and high-emission areas

To reveal the spatial characteristics of building carbon emissions in Guangzhou, the calculated results were allocated to a 100 m × 100 m grid. Specifically, each building's total carbon emissions were assigned to the grid cell containing the centroid of its footprint, and the emissions of all buildings whose centroids fell within the same grid cell were summed to obtain the carbon emission value of that cell. Based on the aggregated grid-level results, the natural breaks method was applied to classify carbon emission levels into five categories, and a gridded carbon emissions map was generated (Fig. 5(a)). In addition, a kernel density analysis was conducted to identify the spatial clustering of carbon emissions (Fig. 5(b)). The former illustrates the hierarchical differences in carbon emissions levels across the city, while the latter highlights the degree of spatial concentration of high-emission zones.

As shown in Fig. 5(a), the spatial distribution of building carbon

Table 14
Carbon emission characteristics of different districts.

District	Total carbon emissions ($WtCO_2e$)	Percent	Area (km^2)	Carbon emissions (tCO_2/km^2)
Liwan	6950	6.9%	59	118
Yuexiu	6940	6.9%	34	205
Haizhu	12,843	12.7%	90	142
Tianhe	13,073	12.9%	96	136
Baiyun	25,593	25.3%	796	32
Huangpu	7729	7.6%	484	16
Panyu	19,375	19.2%	530	37
Huadu	8667	8.6%	970	9

Table 15
Characteristics of carbon emissions from buildings of different ages.

Age range	Total carbon emissions ($WtCO_2e$)	Percent	Carbon emissions ($kgCO_2e/m^2$)
Pre-1980	2373	2.2%	1405
1980–1984	2844	2.6%	2005
1985–1989	4960	4.5%	1772
1990–1994	12,171	11.0%	1738
1995–1999	26,731	24.2%	1754
2000–2004	37,190	33.7%	1755
2005–2009	10,832	9.8%	1800
2010–2014	6988	6.3%	1826
2015–2020	6259	5.7%	1874

emissions exhibits a clear hierarchical pattern across Guangzhou. Grids of Level 1 and Level 2 account for 46.5% and 35.1% of the total, respectively, indicating that most areas of the city are characterized by relatively low emission levels. In contrast, Level 4 and Level 5 grids comprise only 3.7% and 0.6%, respectively.

The kernel density analysis further reveals evident spatial clustering patterns of emissions (Fig. 5(b)). Core high-density emission zones are concentrated in the central urban area, with secondary hotspots extending along the city's primary development axes—forming a continuous corridor linking Yuexiu, Tianhe, and Haizhu districts, and further extending northwards to southern Baiyun District and eastwards to western Huangpu District. This configuration forms a distinct north–south high-emission belt, highlighting the city's pronounced banded distribution of carbon intensity. Overall, the spatial morphology of building carbon emissions in Guangzhou can be characterized as "central concentration with peripheral dispersion".

3.3. Spatial distribution of carbon emissions by building type

Building types across Guangzhou were allocated to 100 m × 100 m grids to examine the spatial distribution of different building functions throughout the city. During the reclassification process, the following principle was applied: if one building type occupied the largest proportion of built-up area within a grid, that grid was fully assigned to that building type. As shown in Table 16, residential buildings accounted for the largest share of all grids (32%), followed by industrial buildings (32%) and educational and cultural buildings (13%).

The various building types exhibit markedly distinct spatial clustering patterns across Guangzhou. To further identify the spatial aggregation characteristics of major functional building categories, a kernel density analysis was conducted for residential, industrial, office, and commercial buildings (Fig. 6).

Residential buildings are widely distributed, forming continuous belt-shaped clusters. High-density residential areas are concentrated in the central urban districts and gradually weaken toward the outer suburbs, yet still radiate outward along major development corridors. Industrial buildings show a multi-nodal clustering pattern at the periphery of the city, with hotspots primarily located in non-central districts, reflecting the city's trend of industrial relocation and industrial-park agglomeration. Office buildings demonstrate the most prominent "central single-core" clustering, concentrated in the central business district (CBD), indicating a high concentration of commercial and administrative functions. The spatial distribution of commercial buildings is similar but more extensive, with secondary clusters emerging in some outer districts.

Educational and cultural buildings are mainly located in historic central areas but also form secondary high-density clusters in newly developed university towns, producing a "traditional old city + emerging campus" dual-core structure. Medical buildings present a multi-centered pattern characterized by "central concentration with regional diffusion": while core clusters remain in traditional urban centres such as Yuexiu, Tianhe, and Haizhu District, new hotspots have

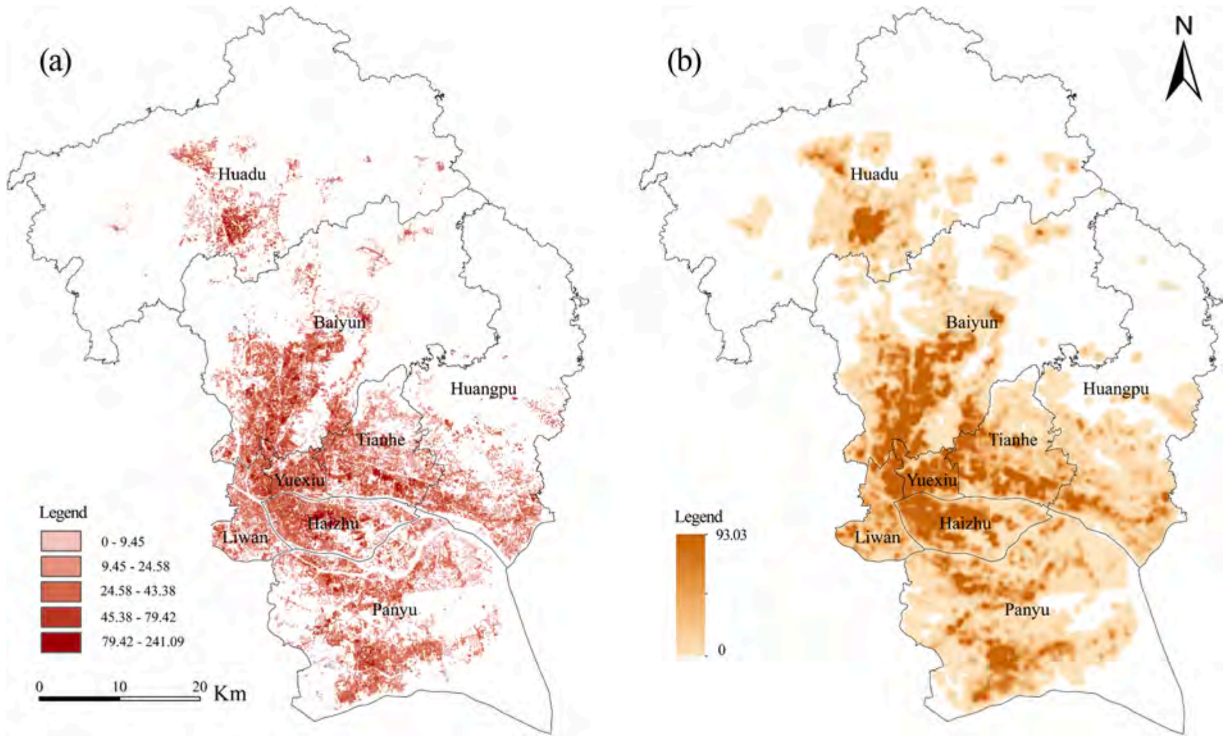

Fig. 5. (a) Spatial distribution of building carbon emissions in Guangzhou on a 100 m grid (Kt); (b) Carbon emission kernel density distribution map (Kt).

Table 16
Number and proportion of building type grids in Guangzhou City.

Building type	Residential	Factory	Office	Commercial	Education and culture	Medical	Others
Number	21,853	21,759	1605	5508	9017	1245	7727
Percent	32%	32%	2%	8%	13%	2%	11%

also emerged in outer districts including Panyu and Huadu District, reflecting an ongoing decentralization of medical resources. Buildings categorized as "other uses" are more scattered and lack distinct clustering, with their spatial characteristics remaining relatively diffuse.

The carbon emissions associated with different building types vary significantly among Guangzhou's administrative districts (Fig. 7). Residential buildings dominate total carbon emissions in Yuexiu (58%) and Baiyun District (44%), highlighting their primarily residential function—particularly in Yuexiu, which retains the characteristics of a traditional dense residential district. In most other districts, residential buildings remain the largest contributors to carbon emissions, though with considerable variation; for instance, in Tianhe District, the share is only 34%. Industrial buildings contribute most prominently to carbon emissions in Huangpu (53%), Panyu (34%), and Huadu District (24%), confirming the city's pattern of industrial concentration in peripheral areas.

Office and commercial buildings account for a higher proportion of carbon emissions in Tianhe and Haizhu districts, reflecting their predominantly service-oriented urban functions. Furthermore, educational and cultural buildings in Tianhe District account for 26% of its total emissions, highlighting its role as an educational and cultural hub, with numerous schools, libraries and cultural institutions located within the district.

From the perspective of distributional characteristics (Fig. 8), residential buildings exhibit higher-value grids particularly in Yuexiu, Haizhu, and Huadu, with Yuexiu District showing the most persistent high-value concentration. Industrial emissions are dominated by low-value grids, with few high-value occurrences across districts. Office buildings display a wider distribution curve concentrated in high-value ranges, indicating greater spatial variability. Commercial and medical buildings show similar patterns but with more extreme high-value grids and higher overall peaks. In contrast, educational/cultural and other building types maintain lower overall emission levels and exhibit smaller inter-district differences.

3.4. Spatial distribution characteristics of building age and associated carbon emissions

The spatial distribution of building floor area in Guangzhou across three construction periods—before 1989, 1990–2004, and 2005–2020—at a 100 m grid resolution is shown in Fig. 9.

Buildings constructed before 1989 were concentrated in the traditional central districts, with the highest densities found in Yuexiu, Liwan, and Haizhu District, corresponding to Guangzhou's historical urban core. This pattern indicates that urbanization before 1989 was primarily confined to the core area, without significant outward expansion. During 1990–2004, the city entered a period of rapid urban expansion, with high-density development spreading toward Tianhe, Baiyun, Panyu, and Huangpu Districts. Notably, Tianhe District exhibited a sharp increase in building density, consistent with its emergence as Guangzhou's secondary city center and major commercial development zone. From 2005 to 2020, intensive growth occurred along the urban periphery, as high-density building clusters extended further into Panyu and Huadu District, reflecting the city's continuous outward expansion toward new suburban centers. However, some of these newly developed zones may feature high building density but low occupancy, implying potential high carbon emissions coupled with low utilization rates, such as elevated vacancy levels.

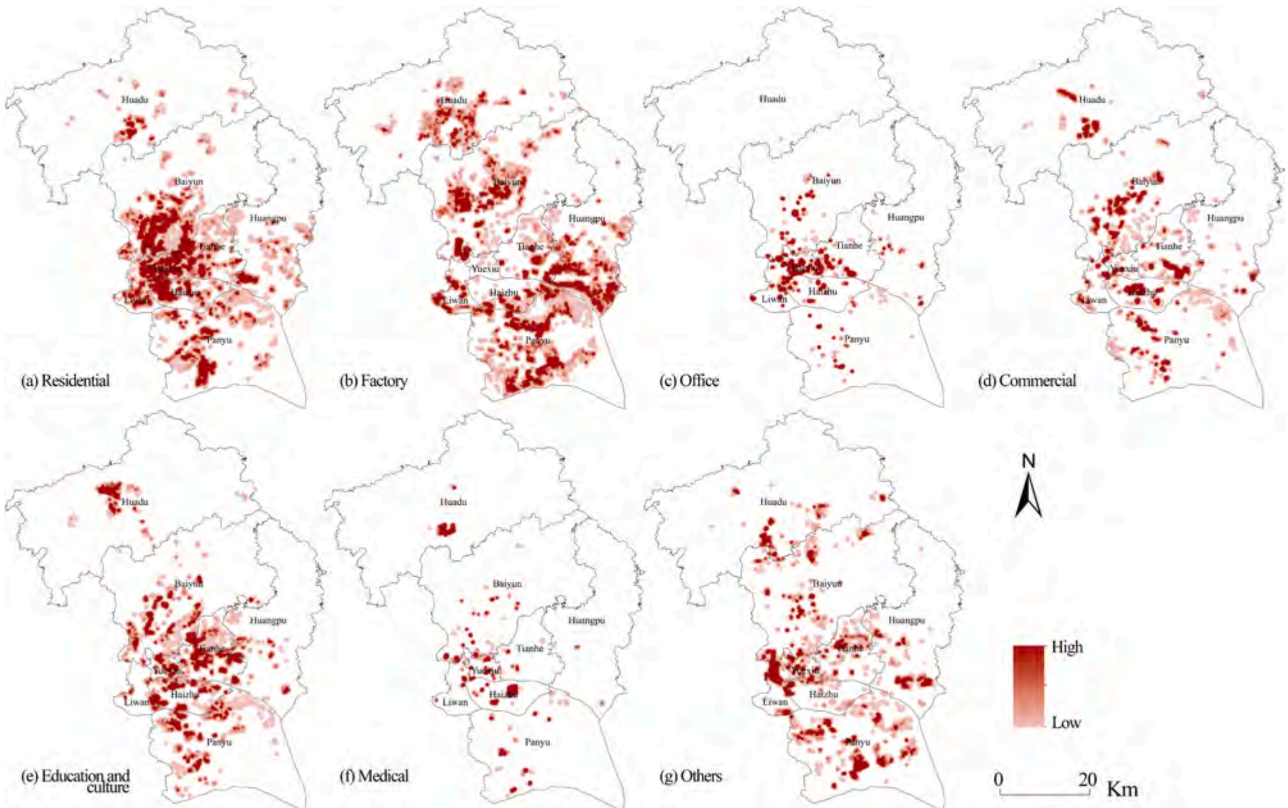

Fig. 6. Distribution of nuclear density by building type.

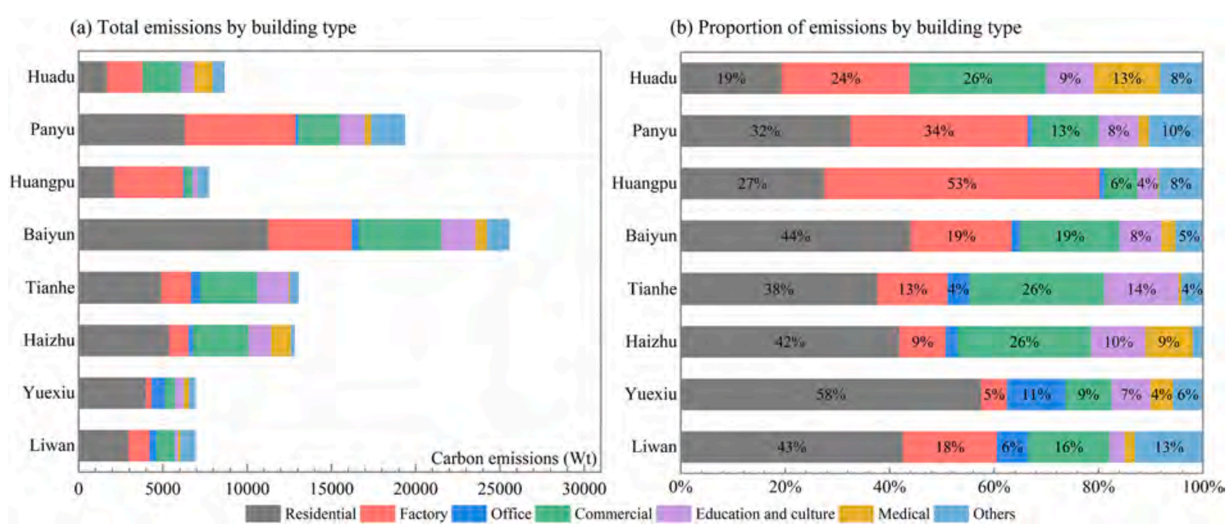

Fig. 7. Building carbon emissions by type across districts in Guangzhou.

To further analyze the spatiotemporal dynamics of carbon emissions, this study examined how buildings from different construction periods contribute to emissions across various life-cycle stages and time intervals. Assuming a 35-year operational lifespan, carbon emissions from material production, transport, and construction were allocated to the year of completion, while operational carbon emissions were distributed annually over the subsequent 35 years, and demolition carbon emissions were assigned to the final year of the life cycle. Following this approach, the spatial kernel density maps of building-related carbon emissions for different time periods were generated (Fig. 10).

Buildings constructed before 1979 produced small and scattered emission hotspots, primarily concentrated in Yuexiu's old urban core and the industrial belt along the river in Liwan District, consistent with Guangzhou's early urbanization pattern characterized by fragmented and low-density emissions.

Between 1980 and 1994, distinct high-density emission clusters emerged in Yuexiu, Tianhe, southern Baiyun, and northern Haizhu District, indicating a substantial increase in construction during this period. These buildings are now in their mid- to late life-cycle stages, with ongoing operational emissions superimposed upon earlier embodied emissions, resulting in intensified spatial hotspots.

The period 1995–2009 represents one of the most carbon-intensive phases in Guangzhou's building history, featuring the largest and strongest hotspots. Core emission zones remained in Yuexiu, Haizhu,

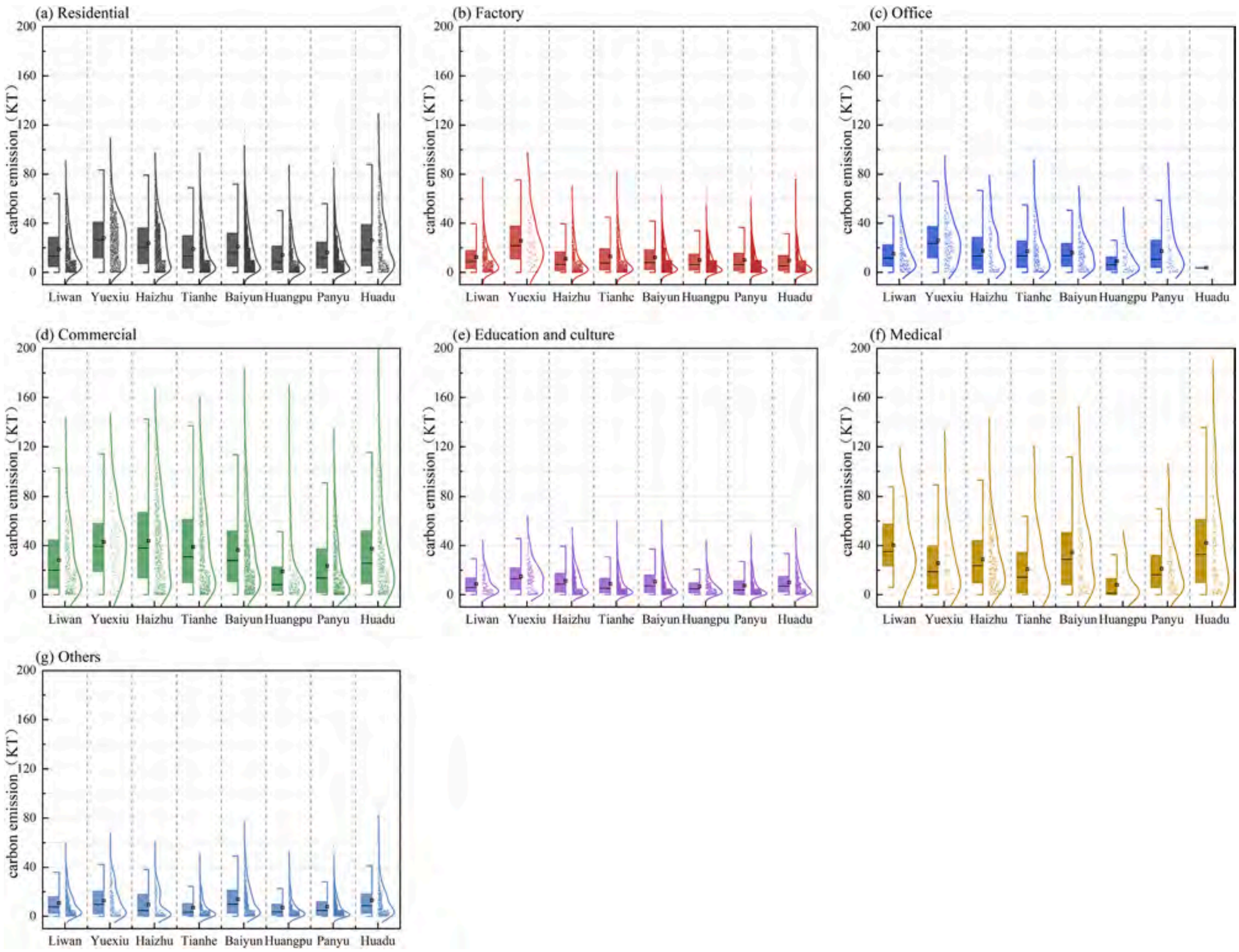

Fig. 8. Distribution of carbon emissions per building type across administrative districts (Boxes represent the 25th, 50th, and 75th percentiles; whiskers indicate the minimum and maximum values within 1.5 times the interquartile range (IQR) from the box edges).

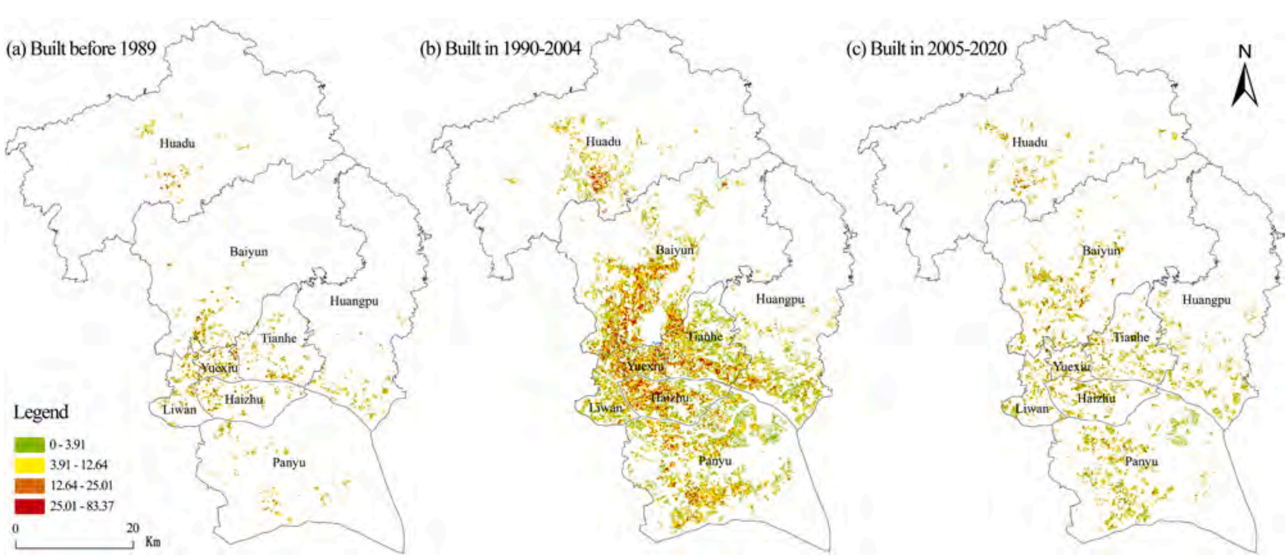

Fig. 9. Spatial distribution of building floor area in Guangzhou across different periods (10^3m^2/grid).

and northern Tianhe District, while peripheral districts such as Panyu, Huangpu, and Huadu began to show increasing carbon emission pressures. This corresponds to Guangzhou's most rapid phase of urban expansion, when dense new construction coincided with the onset of major operational emissions from buildings completed in previous years.

For 2010–2024, representing the current period, emission intensity has shown a slight decline, with hotspots becoming more concentrated.

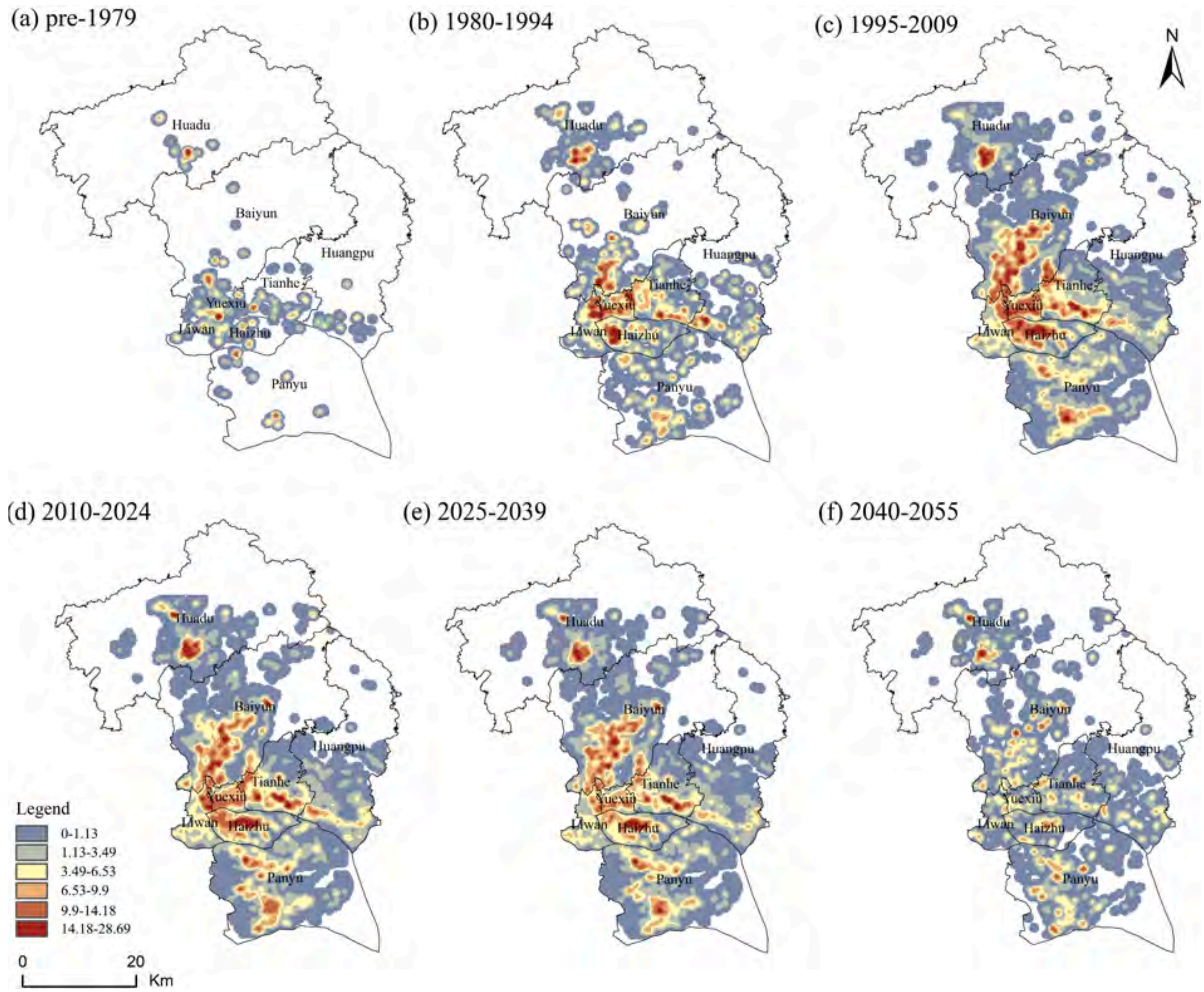

Fig. 10. Spatial distribution map of carbon emissions from existing buildings in Guangzhou by year (KT).

However, these remain predominantly located in central urban districts, northern Panyu, and Huangpu. These areas are characterised by high building density and intensive energy usage.

The projection for 2025–2039 reflects the continuing operational emissions from existing buildings over the next 15 years. The spatial distribution of hotspots remains similar to that of 2010–2024, but with reduced intensity as some buildings approach the end of their life cycles.

By 2040–2055, emission hotspots decrease significantly, breaking into smaller, fragmented clusters. Isolated hotspots appear in the outer districts, while most central areas exhibit a marked decline in emission density. The hotspots retreat toward the urban fringes, dominated by residual operational emissions and demolition-related carbon releases in the final years of the life cycle.

Overall, emission hotspots within Guangzhou's existing building stock exhibit a dynamic temporal evolution: shifting from the city centre towards peripheral areas, before gradually retreating. This trajectory mirrors the city's broader process of urban expansion and density evolution, highlighting that future carbon mitigation efforts should prioritize recently developed high-intensity zones and current operation-dense areas, where emission reduction interventions could yield the greatest impact.

3.5. Material use and recycling potential

Based on the previously established 35-year building lifespan, the study projected the material use, recycling potential, and spatial distribution of demolition materials in Guangzhou for the next 35 years (2020–2055) (Fig. 11). Overall, the spatial distribution of demolition material potential exhibits a distinct temporal evolution, with demolition intensity peaking in the 2030s and gradually declining thereafter.

During 2020–2029, Guangzhou's potential for recovered demolition materials remains generally low and spatially scattered, primarily concentrated in the urban core and a few early-developed peripheral zones, such as Yuexiu, Liwan, Haizhu, and parts of Tianhe District. Most grids exhibit potential values below 100 kilotons, with only a few core areas (e.g., Yuexiu) reaching 100–1000 kilotons. This suggests that demolition during this period is largely limited to isolated renewal of aging buildings, rather than large-scale urban renewal waves.

Between 2030 and 2039, the volume of recoverable materials increases significantly and becomes more widely distributed, marking the peak demolition decade among the four analyzed periods. Extensive high-value regions emerge, particularly across Baiyun, Panyu, Tianhe, and Huangpu Districts, indicating that many buildings in these areas will have reached the end of their service life and are likely to enter demolition cycles. Suburban expansion belts beyond the central city also display substantial recycling potential, suggesting that developments from the late 1990s and early 2000s are now approaching the renewal phase.

During 2040–2049, the demolition intensity declines slightly compared to the previous decade but remains at a moderate level. Recycling potential becomes concentrated in outer districts such as Panyu and Huadu Districts, though the intensity distribution shifts toward medium-to-low levels. This phase primarily involves buildings constructed around 2005, reaching the 35-year end-of-life threshold,

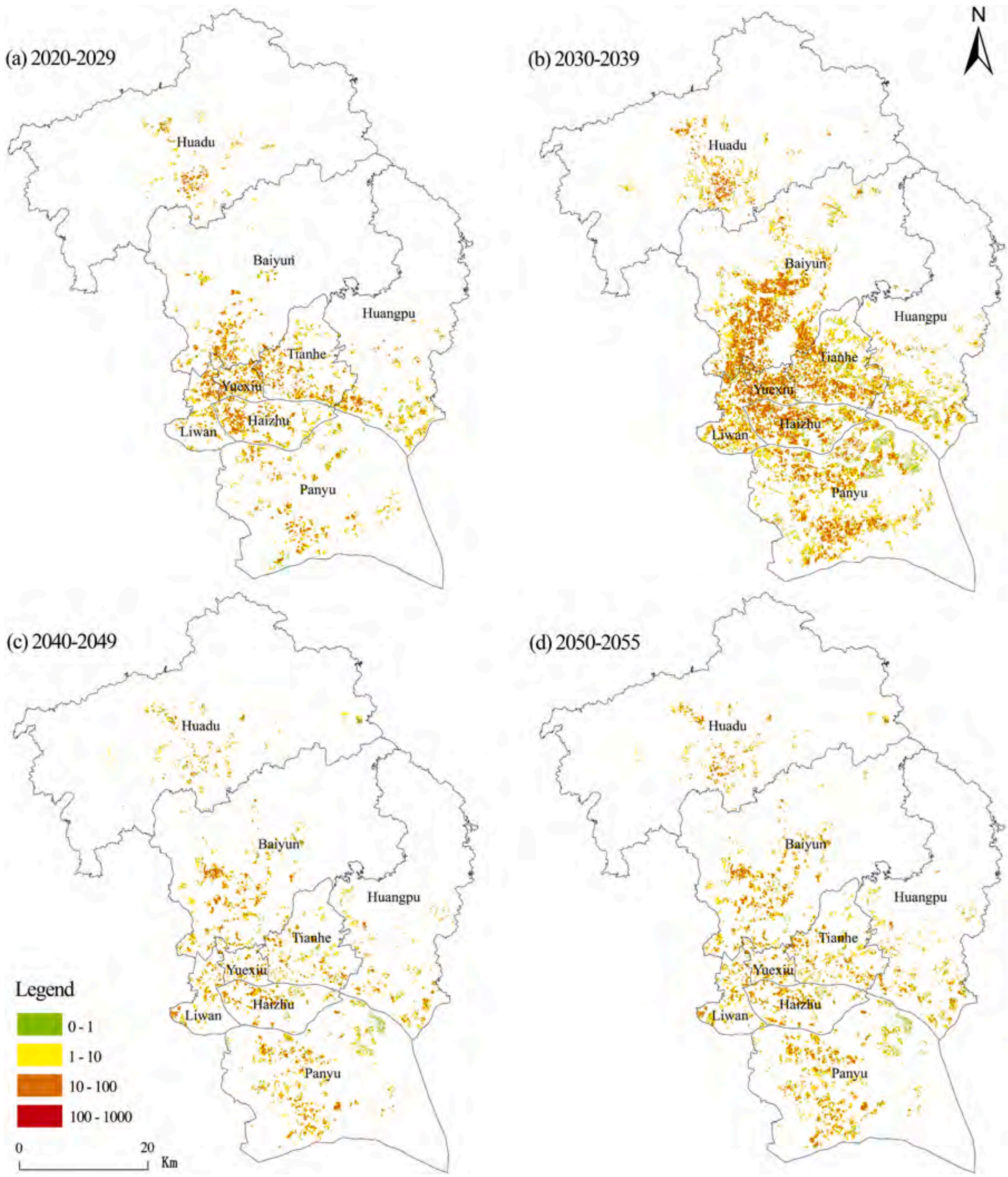

Fig. 11. Spatial distribution map of building material stockpiles for demolition in Guangzhou at different time periods (KT).

corresponding to the second wave of suburban expansion. Meanwhile, demolition activity in the central districts decreases sharply, as urban renewal of the old core has been largely completed in earlier decades.

By 2050–2055, the potential for demolition materials declines further, entering a relatively stable phase. The spatial distribution becomes more dispersed, dominated by low-intensity areas with only sporadic medium-level hotspots. The pace of building renewal stabilizes, signalling a shift from large-scale construction to maintenance and localized renovation. Most potential recycling activities are expected to occur in later-developed peripheral districts such as Huadu and Panyu District.

Fig. 12 presents the projected quantities of demolition material stocks for Guangzhou and its eight major administrative districts across different periods, further disaggregated into eight primary material categories. Temporally, nearly all districts are projected to reach their peak demolition material reserves during 2035–2039, followed by secondary peaks before 2029 and between 2040 and 2044. This pattern reflects the concentrated wave of urban construction in the early 21st century, with this generation of buildings expected to enter large-scale demolition between 2035 and 2044, thereby creating a significant surge in recoverable materials.

In terms of material composition, brick and sand constitute the largest shares, followed by cement and stone, while asphalt and glass contribute only minor proportions. Traditional central districts such as Yuexiu and Liwan are projected to reach their demolition material peaks before 2029, indicating a predominance of aging building stock and an earlier demolition timeline compared with newer suburban areas. In contrast, Huadu, Huangpu, and Panyu District exhibit a more balanced

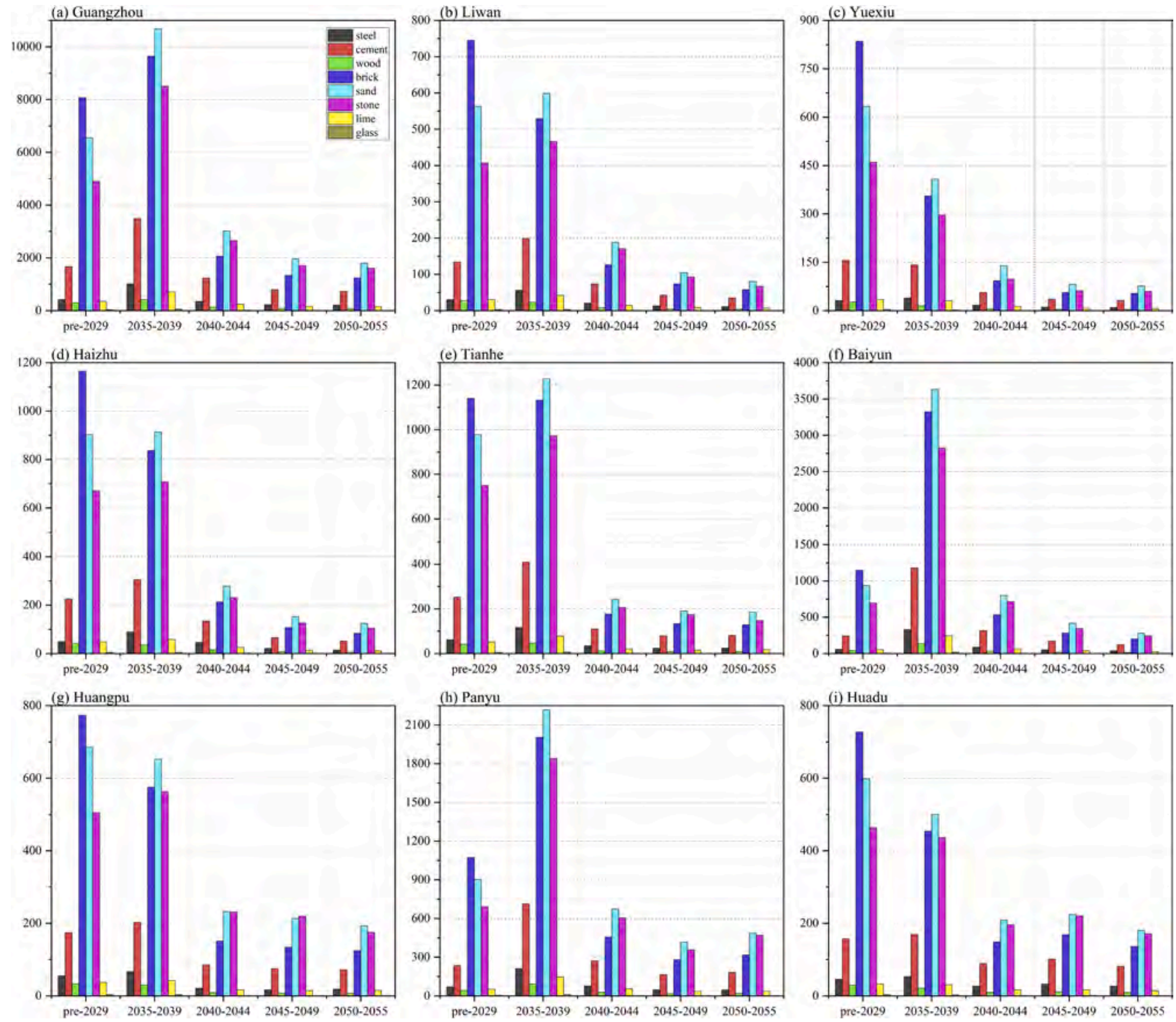

Fig. 12. Projected material stockpiles for buildings scheduled for demolition in each district during different periods.

and delayed demolition pattern, with their demolition peaks likely occurring after 2045.

3.6. Relationship between building carbon emissions, population, and economy

To investigate the spatial coupling between building carbon emissions and socioeconomic factors, this study employed 1 km–resolution grid data for Guangzhou to construct scatterplot regression models between building carbon emissions and both population density and GDP density, analyzing their correlations at both the citywide and district scales (Fig. 13).

At the citywide scale, building carbon emissions show a moderately strong positive correlation with population density ($R^2 = 0.66$), indicating that carbon emissions are spatially concentrated in areas of high population density. In contrast, the correlation between carbon emissions and GDP density is much weaker ($R^2 = 0.16$), suggesting limited spatial alignment between economic output and building-related emissions.

At the district scale, most administrative areas exhibit a significant positive correlation between building carbon emissions and population density. Among them, Liwan District shows the steepest regression slope ($Y = 15.49X + 2663.47$, $R^2 = 0.77$), implying high population density per unit of building-related carbon emissions and reflecting its dense residential character as an old urban district. Other districts, including Yuexiu ($R^2 = 0.61$), Tianhe ($R^2 = 0.70$), Baiyun ($R^2 = 0.67$), Panyu ($R^2 = 0.63$), and Huadu ($R^2 = 0.62$), also demonstrate strong correlations, confirming that building carbon emissions are primarily driven by residential population size.

In contrast, the relationship between building carbon emissions and GDP density is generally weaker, showing only a moderate positive correlation in Tianhe District ($R^2 = 0.36$)—likely due to its role as Guangzhou's business and financial hub, where economic output aligns closely with dense building activities. In Huangpu ($R^2 = 0.09$) and Baiyun ($R^2 = 0.09$), districts dominated by industrial or logistics functions, building carbon emissions remain high but are spatially decoupled from GDP, suggesting a mismatch between energy consumption and economic productivity.

Overall, at the 1 km resolution, building carbon emissions in Guangzhou are highly consistent with population distribution but less correlated with GDP distribution, indicating that residential activities, rather than economic output, are the dominant spatial drivers of building-related carbon emissions.

Building upon these regression results, a tertile-based bivariate

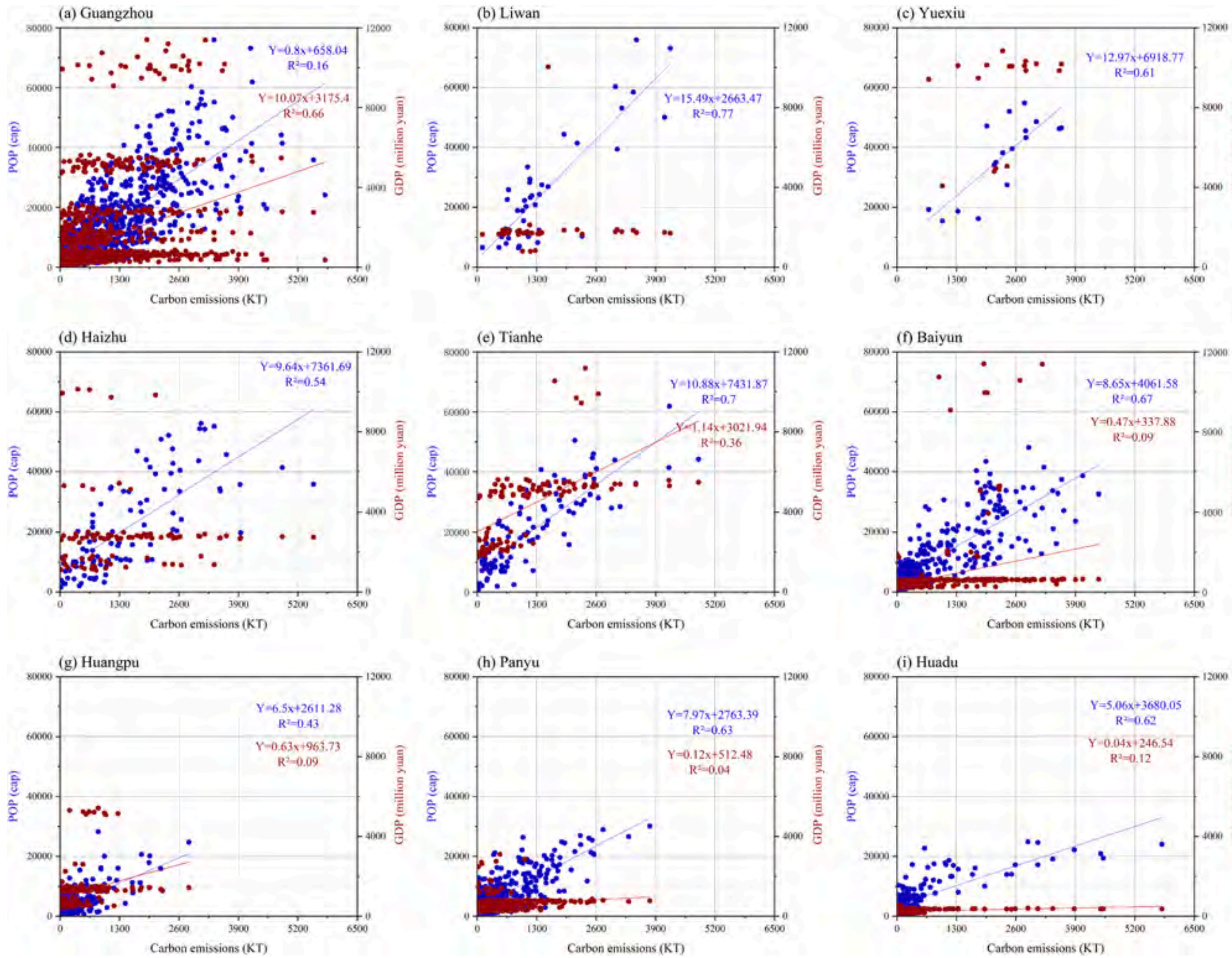

Fig. 13. Correlation between building carbon emissions and population-economic factors in Guangzhou City and its districts (Note: Districts without regression equations or fitted trend lines indicate statistically insignificant correlations ($p > 0.05$)).

classification was performed to further examine the spatial coupling between carbon emissions and population/GDP density. Both carbon emission intensity and socioeconomic variables were divided into three levels (low, medium, high), and cross-classified into nine spatial combination types (Fig. 14). Fig. 14(a) shows the carbon–GDP classification, while Fig. 14(b) depicts the carbon–population bivariate classification. In the legend, the first digit represents the carbon emission level (1 = low, 2 = medium, 3 = high), and the second digit indicates the population or GDP density level (1 = low, 2 = medium, 3 = high). This approach identifies representative coupling types such as “high-carbon–high-population”, “low-carbon–high-population”, and “high-carbon–low-GDP”. The resulting proportions of these nine categories for different building attributes and districts are presented in Fig. 15.

Figs. 14 and 15 together reveal pronounced spatial heterogeneity in the coupling patterns across Guangzhou’s districts. The “high-carbon–high-population” (3, 3) type is primarily concentrated in central districts such as Haizhu, Yuexiu, and Liwan, whereas “high-carbon–low-GDP” and “high-carbon–medium-GDP” types are clustered in peripheral districts like Baiyun and Huadu, reflecting notable spatial inefficiencies in carbon emission performance.

Fig. 15 further quantifies the relative shares of the nine bivariate spatial types by administrative district. The central districts (Yuexiu, Liwan, Haizhu) are dominated by “high-carbon–high-population” or “high-carbon–high-GDP” combinations, illustrating areas where dense population and high economic output coincide, forming the city’s core carbon-emission zones. Tianhe District exhibits a diversified structure, with both “high-carbon–high-population” and “medium-carbon–high-population” types, reflecting its mixed residential–commercial character. In contrast, peripheral districts—such as Baiyun, Panyu, Huadu, and Huangpu—show more dispersed and heterogeneous patterns, including “medium-carbon–low-population”, “low-carbon–low-population” and localized “high-carbon–low-population” or “high-carbon–medium-GDP” grids, indicating a spatial decoupling between carbon emissions and both population and industrial output in expanding suburban zones.

At the building-type level, residential buildings show the highest proportion of the “high-carbon–high-population” type, underscoring the strong spatial coupling between housing emissions and population density. Office buildings are almost entirely categorized as “high-carbon–high-population” or “high-carbon–high/medium-GDP” types, representing carbon-intensive but economically productive zones. In contrast, educational/cultural and industrial buildings are mostly characterized by medium- or low-carbon types, with lower carbon emission intensities and more balanced spatial use.

From the temporal perspective, pre-1989 buildings are predominantly found in “high-carbon–high-population” and “high-carbon–high-GDP” zones, reflecting the intensive, compact nature of the historical city core. Buildings constructed between 1990 and 2004 exhibit a more dispersed spatial pattern, with increased proportions of “medium-carbon–high-population/GDP” grids, reflecting outward urban expansion. The 2005–2020 building cohort is largely associated with “low-carbon–low-population” or “low-carbon–low-GDP” zones, indicating that

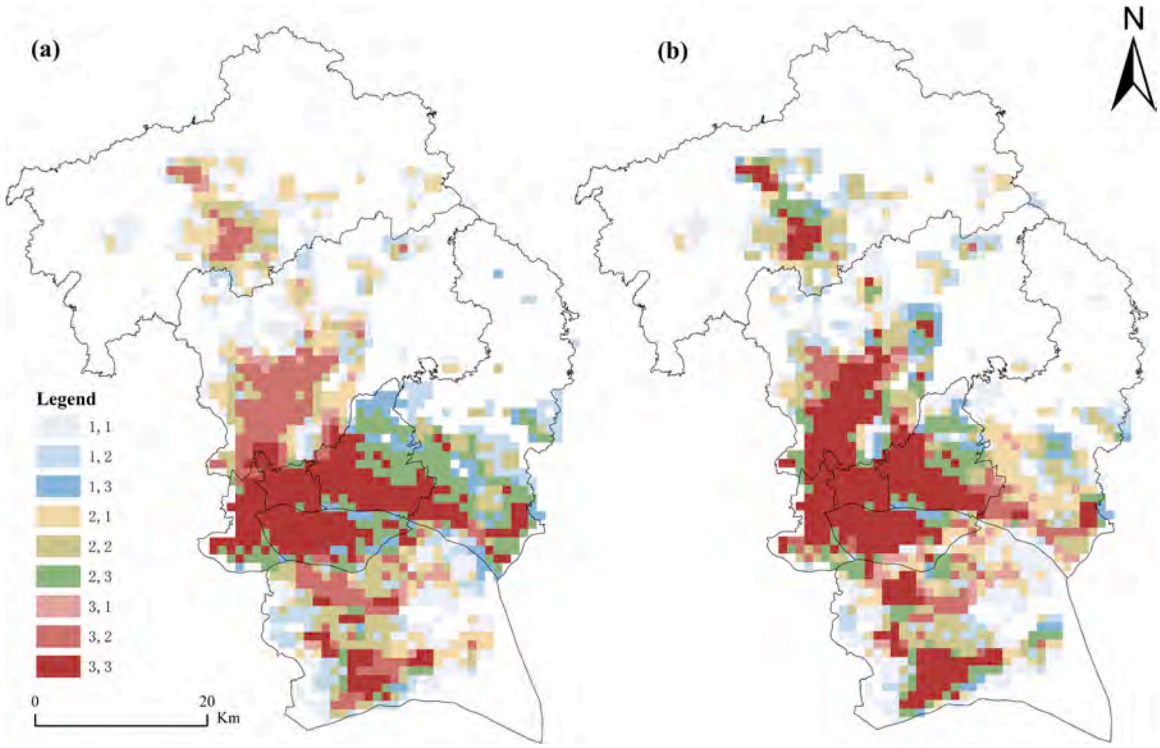

Fig. 14. Bivariate classification map of carbon emissions and GDP / population density.

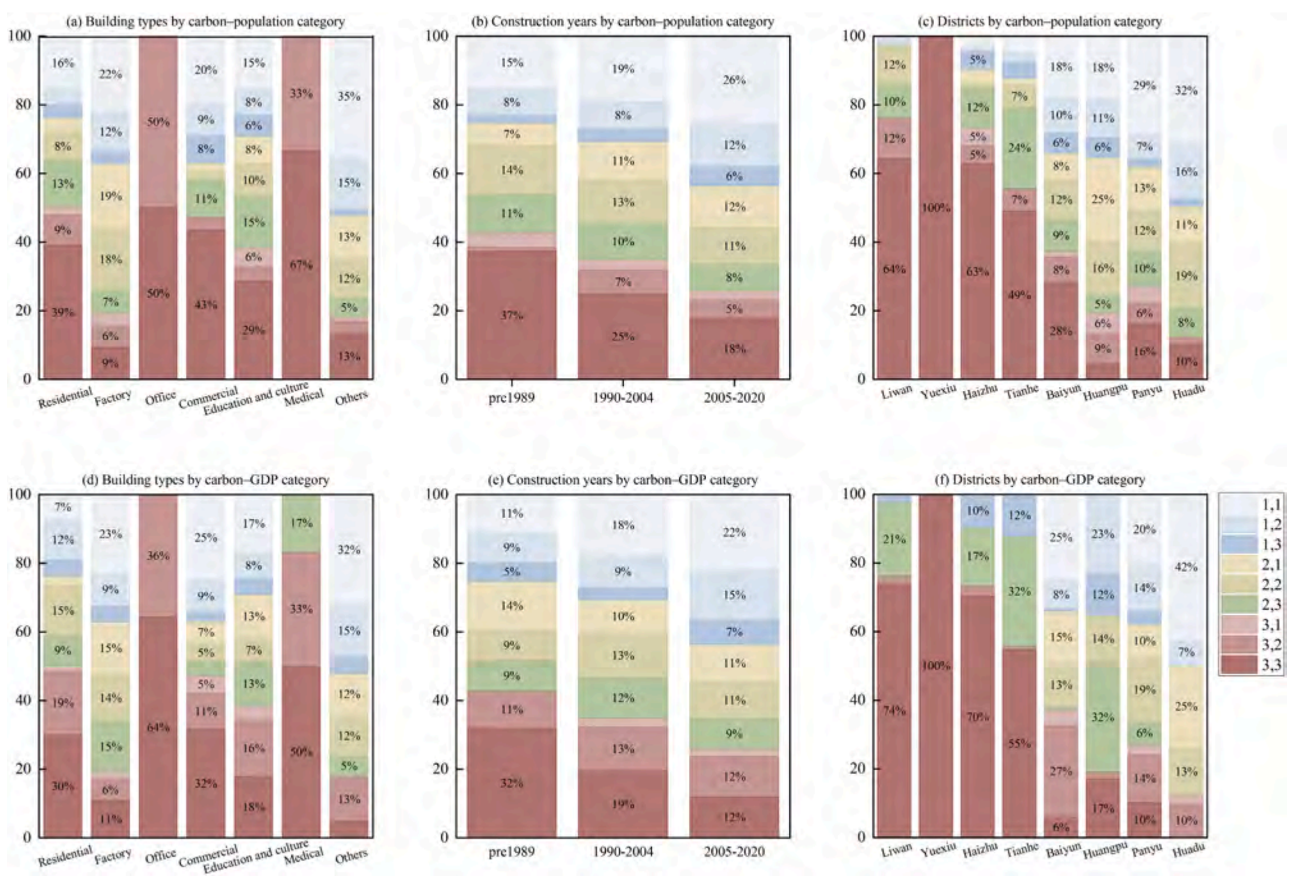

Fig. 15. Distribution of building characteristics under different carbon–population and carbon–GDP spatial categories in Guangzhou.

new construction is concentrated in low-density peripheral areas, consistent with the city's urban sprawl trend.

In summary, Guangzhou's spatial structure of building carbon emissions demonstrates a pattern of "high coupling and efficiency in the core, low efficiency and decoupling in the periphery." In central districts, building carbon emissions are tightly linked to population and economic activity, while in newly developed outer districts, there exists a clear decoupling between building carbon emissions, population, and GDP, suggesting uneven carbon efficiency across the urban landscape.

4. Sensitivity and uncertainty analysis

4.1. Uncertainty analysis of intra-group variation in the MCI

The total carbon emissions changed by 0.06% under the minimum scenario and by 0.07% under the maximum scenario. Table 17 presents the rates of change for major carbon emissions under different classification scenarios; the complete table and summary results are provided in Support information 2.

The MCI sensitivity analysis reveals that the overall variation in total building carbon emissions is limited, ranging from 3.16% to 3.17%. Among material categories, bricks and glass contribute most to the variation, whereas the effects of cement, timber, and lime are negligible. Spatially, the magnitude of variation across regions is generally small, mostly within ±0.4%. However, differences are more pronounced among construction periods, particularly for buildings constructed in 1985–1989 and 2015–2020, indicating that MCI uncertainty has a more notable influence on specific age cohorts than on regions or building types.

Because the construction-period dimension showed relatively larger variation in the MCI sensitivity analysis, this study further examined the carbon-emission change rates of different building-age groups using heatmap analysis (Fig. 16). The results indicate that the influence of MCI uncertainty is mainly concentrated in the material production and transportation stages. From the administrative-district perspective, the change rates in all districts remain generally low, although some inter-period differences can still be observed. The 1985–1989 building group exhibits relatively higher variation across multiple districts, suggesting that the higher sensitivity of this age group is not driven by an anomaly in any single district, but reflects a more widespread pattern. Among building types, residential, industrial, commercial, medical, and other buildings show relatively pronounced changes in certain age groups, whereas educational and cultural buildings exhibit much weaker variation overall. This suggests that the impact of MCI uncertainty on building types mainly depends on the material composition and building-area distribution of that type within specific construction periods.

Fig. 17 illustrates the spatial distribution of the maximum grid-cell change rate of building carbon emissions under the MCI sensitivity scenarios. Specifically, this study calculates the change rate of each 100 m grid cell relative to the baseline scenario under both the MCI minimum and maximum scenarios, and selects the result with the larger absolute magnitude of change as the maximum change rate for that grid cell, in order to characterize the maximum spatial perturbation potentially induced by MCI parameter uncertainty. The results indicate that the change rate of most grid cells is <10%, suggesting that MCI uncertainty does not substantially alter the overall spatial distribution pattern of building carbon emissions in Guangzhou. Locally sensitive grid cells are predominantly distributed in parts of Yuexiu, Haizhu, and Tianhe Districts, where building stock is dense and the composition of building ages and building types is relatively complex, thus exhibiting a more pronounced response to changes in material consumption intensity. Overall, MCI uncertainty primarily induces fluctuations at the local grid-cell scale, rather than causing a systematic shift in the spatial pattern.

Overall, this paper concludes that variations within the MCI group do not alter the study's main findings; however, when explaining differences in carbon emissions between buildings of different ages, it should be acknowledged that there is a degree of uncertainty.

Table 17
Rate of change of major carbon emissions under different classification scenarios.

Dimension	Overall range	Most sensitive category	Interpretation
Material (kg)	0.00%–1.24%	Brick / Glass	Total emissions are moderately affected by material intensity settings
District(Co2eq)	−0.33%–0.36%	Panyu / Huadu	District-level results are stable
Building type (Co2eq)	0.00%–0.12%	Residential / Medical	Type-level differences are negligible
Construction period(Co2eq)	−4.42%–4.41%	1985–1989 / 2015–2020	Age cohorts are more sensitive to MCI uncertainty

4.2. Lifespan scenario analysis

Building service life is an important parameter affecting the accounting results of carbon emissions from existing buildings. To examine the influence of lifetime assumptions on the research results, this study further established three alternative building lifetime scenarios of 25, 50, and 70 years, in addition to the baseline scenario of 35 years. The cumulative carbon emissions, annual emission trends, and spatial distribution differences of the existing building stock under different lifetime scenarios were then compared.

In terms of cumulative carbon emissions, the total carbon emissions of the existing building stock varied substantially across the different lifetime scenarios. Under the 25-year, 35-year, 50-year, and 70-year lifetime scenarios, the total carbon emissions were 0.902, 1.079, 1.343, and 1.697 billion t CO_2e, respectively. Compared with the 35-year baseline scenario, cumulative carbon emissions decreased by approximately 16.4% under the 25-year scenario, while they increased by approximately 24.6% and 57.3% under the 50-year and 70-year scenarios, respectively. This difference is mainly attributable to the cumulative effect of operational emissions. When the assumed building lifetime is extended, existing buildings continue to generate operational carbon emissions over a longer period, thereby increasing cumulative emissions within the accounting boundary.

The annual emission trends further indicate that different lifetime assumptions not only affect the magnitude of cumulative carbon emissions, but also significantly alter the temporal distribution of carbon emission release (Fig. 18). Under the shorter lifetime scenario, existing buildings reach the end of their life cycle earlier, and annual carbon emissions decline rapidly after the 2020s, approaching a relatively low level in the 2030s. Under the 35-year baseline scenario, the decline is relatively delayed, whereas the 50-year and 70-year scenarios show a longer emission persistence period.

From the perspective of spatial distribution, the overall spatial pattern of carbon emission hotspots remains relatively consistent across different lifetime scenarios, but their persistence and attenuation processes differ markedly. Support information 3 shows that changes in building lifetime do not fundamentally alter the spatial core pattern of carbon emissions from existing buildings. However, as the assumed lifetime increases, the spatial persistence of high-emission areas becomes more pronounced. Under the shorter lifetime scenario, emission hotspots in the central urban area and early-developed districts decline earlier. In contrast, under the 50-year and 70-year scenarios, emission hotspots in the central urban area and some peripheral expansion areas persist into later periods. This suggests that longer lifetime assumptions delay the spatial contraction of carbon emissions from the existing building stock.

Overall, the building lifetime sensitivity analysis demonstrates that the lifetime parameter has a significant influence on carbon emission accounting for existing buildings, mainly in three aspects: first, it changes the cumulative operational emissions of the existing building

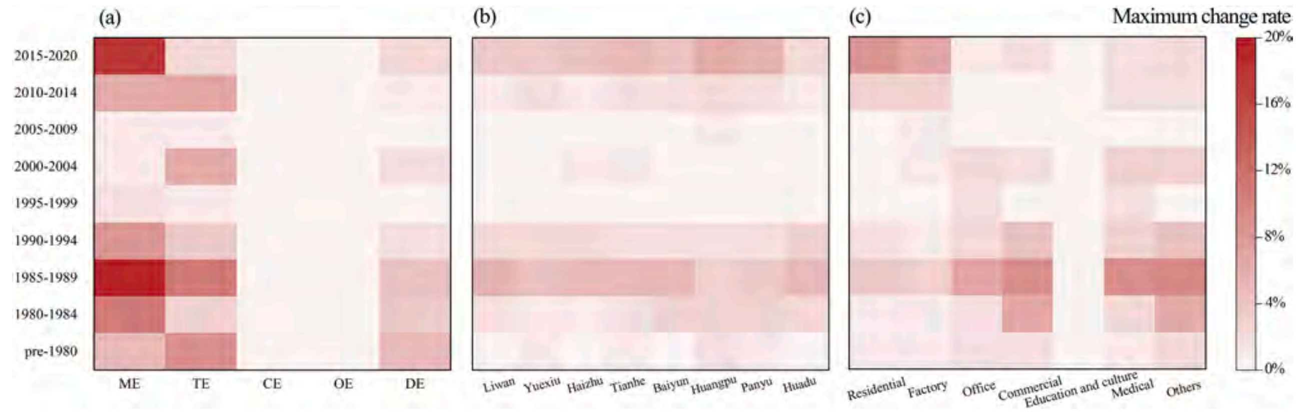

Fig. 16. Heatmaps of maximum carbon-emission change rates by construction period: (a) life-cycle stages, (b) administrative districts, and (c) building types.

stock; second, it alters the decline rate and persistence of annual carbon emissions; and third, it affects the spatial persistence and attenuation process of future carbon emission hotspots.

It should be noted that the lifetime scenario analysis in this study focuses only on the current existing building stock. That is, different lifetime scenarios mainly change the continued operation period of existing buildings and the timing of demolition, without further simulating potential replacement by new buildings after earlier demolition. Therefore, the results of this analysis are primarily used to evaluate the sensitivity of carbon emission accounting results to building lifetime assumptions, rather than to directly determine the absolute emission reduction benefits of shortening or extending building lifetimes within a complete urban renewal process. Future studies aiming to further assess the comprehensive carbon effects of building life extension, early demolition, or renewal and retrofitting should incorporate a dynamic building stock model, integrating demolition, renewal, new construction, and energy-efficiency improvements within a unified analytical framework.

5. Discussion

5.1. Method and innovative significance

This study proposes a city-scale building carbon emission estimation method that integrates multi-source data. Building age was inferred by combining POI data with the KNN algorithm, while building type was determined through the integration of building vector and land-use data. Compared with traditional methods relying on individual building inventories or statistical yearbooks, this approach effectively overcomes the limitations caused by data scarcity, making large-scale, high–spatial-resolution, life-cycle building carbon emission research feasible.

Previous studies on building carbon emissions often exhibit a disconnect between macro and micro-level perspectives: macro-scale analyses based on statistical data can only provide aggregated regional totals (Zhang et al., 2022), while micro-scale studies usually focus on single buildings and thus lack representativeness and scalability (Sim & Sim, 2017). The bottom-up framework proposed in this study for city-scale, life-cycle building carbon emissions analysis integrates both building age and type information, overcoming the infeasibility of individual building inventories and avoiding the lack of spatial resolution inherent in purely macro-level statistical analyses.

Another advantage of this method lies in its universality. As long as basic building vector data and sufficiently detailed POI and land-use data are available, it can be applied to other cities. The required data mainly include the following: (1) building vector data containing geographic coordinates, geometric shape, and height; (2) POI data for inferring building age. In this study, since the selected area is located in and around Guangzhou's central districts, both building and POI information are relatively complete. In China, POI data with construction-year information mainly come from real estate platforms; therefore, the local property market's activity level and online data openness are crucial factors affecting data quality; (3) land-use data for identifying building types, which should contain attributes for different categories of buildings rather than broad classifications such as urban or agricultural land. As POI data improve, the precision and applicability of land-use data related to building types are also increasing; (4) Material Consumption Intensity (MCI) data for estimating material consumption. Although China lacks standardized databases for building material intensity, previous studies have summarized relevant data (Yang et al., 2020); this study compiled these findings into a comprehensive list of material consumption intensity coefficients; (5) parameters for calculating building carbon emissions across life-cycle stages. Previous studies have summarized abundant data on life-cycle building emissions. This research references extensive China-specific literature, fully considering variations in building type and life-cycle phase to ensure accurate results.

The findings from Guangzhou also provide useful references for other cities undergoing similar urban development processes. For example, the concentration of high carbon emissions in old urban districts suggests that existing building retrofits should be prioritized in dense historical cores. The emergence of emission hotspots in peripheral districts indicates that rapid suburban expansion may generate high-carbon and low-efficiency development patterns if population attraction and functional integration are insufficient. In addition, the projected concentration of demolition-related material flows provides a reference for cities facing large-scale building renewal and construction waste management challenges. These findings are particularly relevant for megacities and metropolitan areas in China and other developing regions experiencing intensive urban renewal and outward expansion.

Nevertheless, the direct applicability of this framework depends on local data availability and urban context. POI data quality may vary across cities, especially in areas with less active real estate markets or limited online data openness. Building typology, material intensity, energy consumption patterns, electricity emission factors, and building lifespans also differ by region. Therefore, when applying this framework to other cities, local calibration of key parameters is necessary. Rather than providing a fixed universal result, this study offers a transferable methodological framework that can be adapted to different urban contexts for high-resolution, life-cycle-oriented building carbon emission assessment.

5.2. Results and comparison

This study reveals a distinct spatial pattern of building carbon emissions in Guangzhou, showing an evolutionary trend of "high-carbon

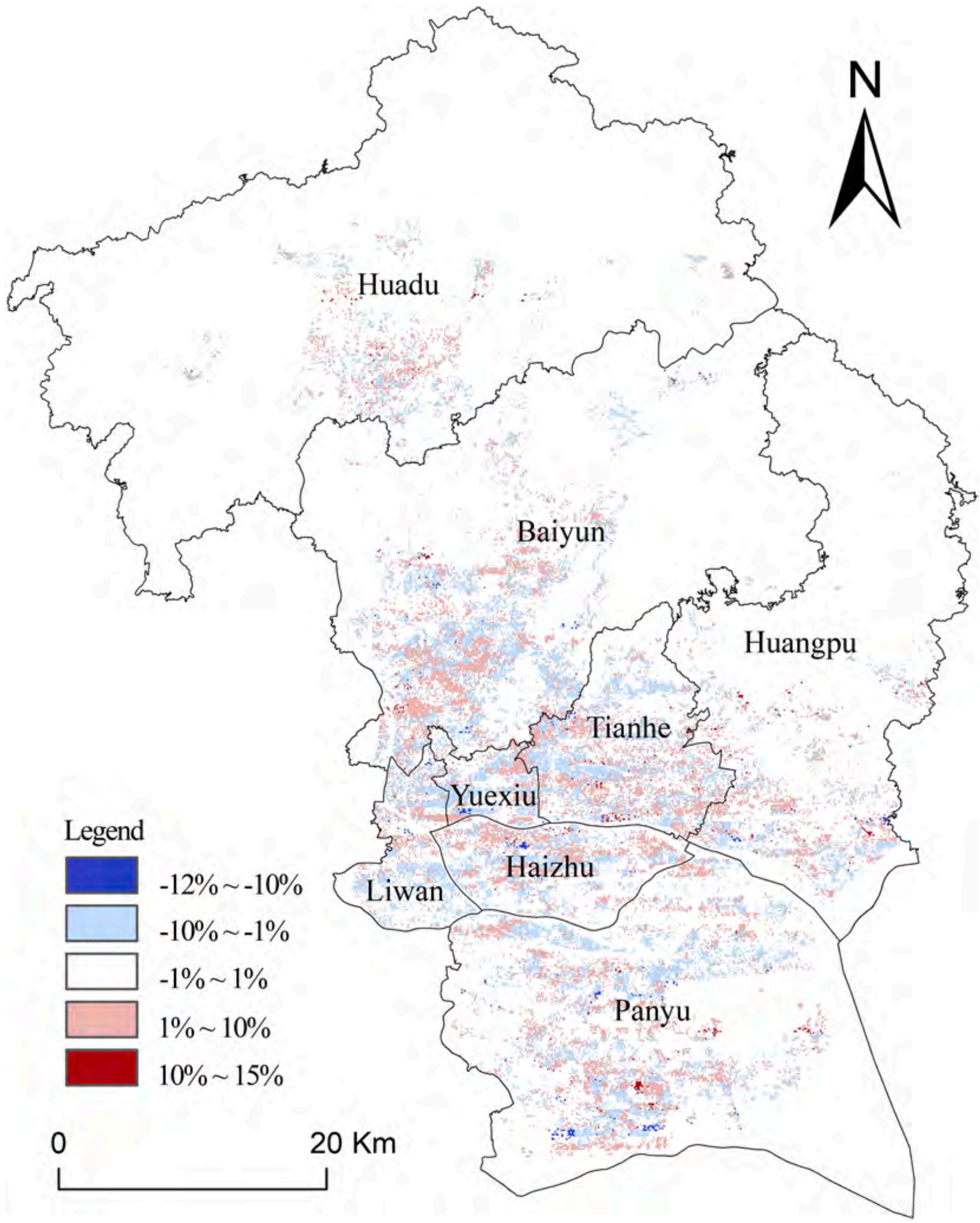

Fig. 17. Spatial distribution of the maximum grid-level change rate in building carbon emissions under MCI sensitivity scenarios.

core–low-carbon periphery–secondary diffusion." Central districts such as Yuexiu, Tianhe, and Haizhu form high-emission clusters, while new hotspots have emerged in Panyu, Baiyun, and Huangpu District due to industrial relocation, university-town construction, and secondary center development. This pattern differs from the "monocentric–polycentric diffusion" structures observed in Beijing and Shanghai, and also from Shenzhen's industrial-park-oriented carbon emission pattern, reflecting the unique industrial transition and multi-center development dynamics of the Pearl River Delta.

It is worth noting that urban building carbon emissions are not solely determined by land-use type but are jointly influenced by spatial morphology, industrial structure, and population distribution. Regarding driving factors, this study finds that population explains building carbon emissions more effectively than GDP, contrasting with the situation in many developed cities where economic activity is the dominant driver. Guangzhou's building carbon emissions are mainly residential-driven: areas of high population density generally correspond to higher building carbon emissions. For example, Yuexiu District, dominated by residential use, exhibits the highest carbon emission intensity per unit area due to its compact urban form and dense population. Conversely, some peripheral areas dominated by industrial buildings have lower emission intensities than central districts. This indicates that land-use classification alone cannot fully explain the spatial differentiation of urban building carbon emissions.

This result aligns with previous studies emphasizing the importance of urban form and spatial structure in influencing carbon emissions (Wang et al., 2017). Given China's heavy decarbonization pressures, carbon emission reduction at the expense of economic development is not a viable path. As high-resolution spatial studies become more prevalent, governments should focus on optimizing urban form and

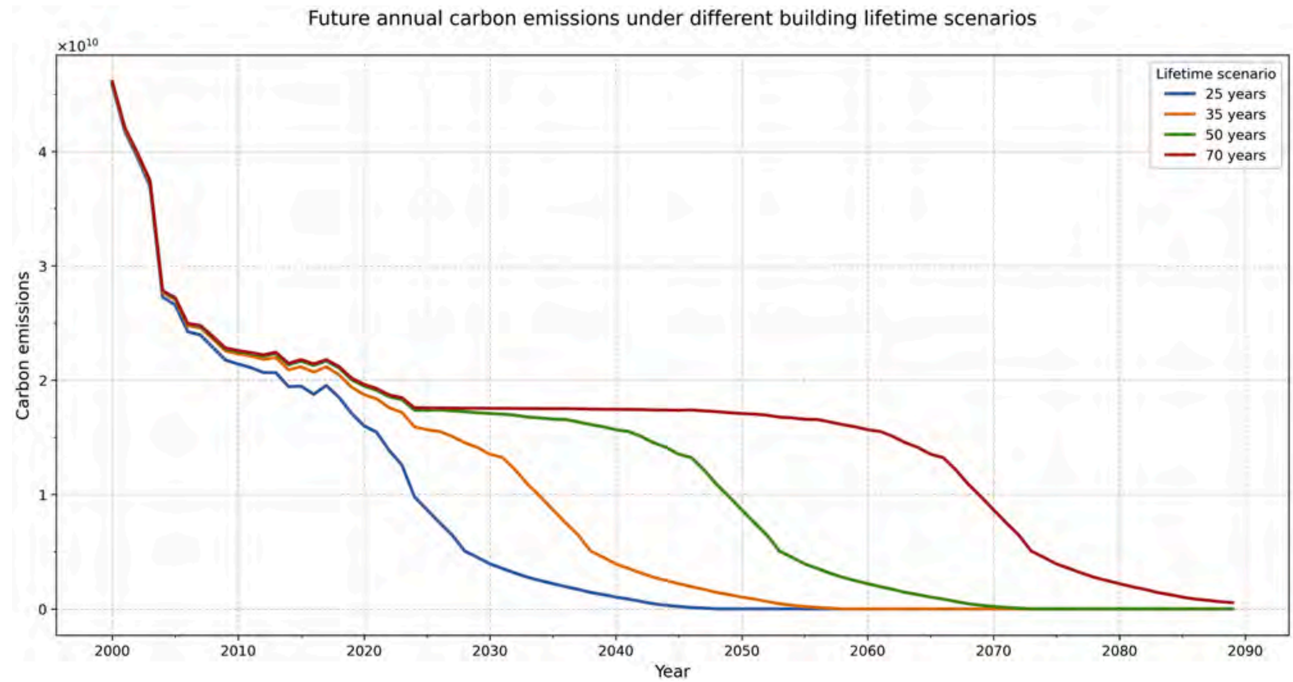

Fig. 18. Annual carbon emission trajectories of existing buildings under different building lifetime scenarios ($kgCO_{2e}$).

spatial structure to achieve carbon reduction while maintaining economic growth—an essential pathway toward the "dual-carbon" goals.

5.3. Policy and practical implications

The results of this study reveal multiple dimensions of Guangzhou's building carbon emissions—spatial distribution, population–economic coupling, and temporal evolution—providing direct insights for urban low-carbon governance and planning.

First, the high-density emissions of old urban districts highlight the importance of existing building retrofits. Core districts such as Yuexiu and Haizhu exhibit far higher carbon emission densities than other areas, dominated by residential and aging public buildings. This finding is consistent with previous studies indicating that "old urban districts have significantly higher building carbon densities than new peripheral areas." Therefore, energy retrofits, green community development, and renewable energy integration should be prioritized over relying solely on energy-efficient new construction.

Second, the study identifies a mismatch between high carbon emissions and low population or GDP in peripheral new districts. This reflects the "high-carbon vacancy" phenomenon observed in other rapidly expanding cities, suggesting inefficiencies in Guangzhou's spatial resource allocation. Without intervention, this decoupling between emissions and productivity may persist. Hence, peripheral areas should strengthen functional integration and population attraction to prevent the emergence of "high-carbon, low-efficiency" development patterns.

Third, the temporal concentration of material recycling potential provides an actionable policy window. This study predicts that 2030–2039 will be the peak period for building demolition and renewal in Guangzhou, with a significant increase in recyclable materials. This finding aligns with domestic and international studies on the "first wave of urban material release". Therefore, governments and industries should proactively develop construction waste management and circular utilization systems to address the emission and waste challenges of the upcoming large-scale demolition wave.

Finally, differentiated carbon reduction pathways across districts deserve attention. The study shows that Guangzhou's districts vary widely in both carbon building emission characteristics and dominant building functions: Tianhe District, dominated by offices and commercial buildings, should focus on reducing operational energy intensity; Huangpu District, dominated by industrial facilities, should emphasize industrial upgrading and energy-efficient technologies; Yuexiu District, dominated by residential buildings, should prioritize energy-efficient retrofits in housing stock. These findings suggest that citywide decarbonization policies should not adopt a "one-size-fits-all" approach but rather tailor strategies to each district's functional role and emission characteristics.

In conclusion, this study reveals the spatiotemporal and functional heterogeneity of Guangzhou's building carbon emissions and provides a practical pathway for low-carbon development: combining old-city retrofitting and energy efficiency improvements, functional optimization and population guidance in new districts, circular material reuse systems, and differentiated emission-reduction strategies by district to achieve coordinated progress in carbon mitigation and urban development.

5.4. Limitations and future outlook

This study still has certain limitations in both methodology and data application. Firstly, although various building lifespan scenarios were introduced to examine the impact of lifespan assumptions, the analysis was limited to the existing building stock. While the different lifespan scenarios altered the duration of continued operation and the timing of demolition for existing buildings, they did not further simulate scenarios such as the construction of new buildings, refurbishment, or changes in operational energy efficiency following demolition. Consequently, the findings should be interpreted as a sensitivity test of lifespan assumptions rather than a comprehensive assessment of the carbon emissions impacts associated with extended building lifespans or early demolition. Secondly, whilst the uncertainty in material consumption intensity (MCI) within each group was examined through sensitivity analysis, the MCI coefficients were still primarily derived from a literature review. The results indicate that variations in intragroup MCI have a limited impact on the overall conclusions, though uncertainty remains for certain building period groups. Consequently, more detailed local material balance data is required to improve the accuracy of carbon emissions accounting for specific building eras, types and regions. Third, the relatively weak correlation found between building carbon emissions and GDP may relate to differences in statistical definitions and scale effects, requiring further exploration.

Future research could proceed in several directions: (1) integrating dynamic urban modelling approaches such as LUCC prediction and BIM-based data to capture building carbon emissions with higher temporal and spatial precision; (2) conducting cross-city comparative studies to evaluate the method's adaptability and robustness under varying urban contexts; and (3) linking analysis with policy scenario simulations, such as carbon trading mechanisms and energy retrofit effectiveness assessments, to provide more practical references for low-carbon urban planning.

6. Conclusion

This study proposes a city-scale framework for mapping whole-life-cycle building carbon emissions at high spatial resolution and applies it to Guangzhou, one of China's most rapidly urbanizing megacities. By integrating building vector data, inferred building age and function, and life-cycle assessment parameters, the study establishes a bottom-up inventory that enables both temporal and spatial characterization of building-related carbon emissions across the urban fabric.

(1) At the aggregate level, the results confirm that Guangzhou's existing building stock represents a substantial carbon burden, with life-cycle emissions dominated by the operation stage, while material production and construction remain non-negligible contributors, especially for newer buildings. Residential, industrial, and commercial buildings together account for the majority of emissions, highlighting that urban carbon mitigation cannot rely on single-sector interventions but must address multiple building functions simultaneously. Moreover, buildings constructed during the rapid expansion period from the mid-1990s to the early 2000s emerge as the main contributors to cumulative emissions, indicating that past urban development decisions continue to shape present and future carbon trajectories.

(2) From a spatial perspective, building carbon emissions exhibit strong spatial heterogeneity and clustering. High-emission hotspots are concentrated in the historic core and major functional centers, characterized by high building density and intensive land use, while peripheral districts display lower average emission intensity but increasingly contribute through large-scale expansion. The spatial evolution of emission hotspots over time reveals a dynamic pattern of outward diffusion during periods of rapid urban growth, followed by partial contraction as buildings approach the end of their operational life. This temporal–spatial coupling underscores the importance of considering urban growth history when identifying priority areas for carbon mitigation.

(3) The analysis further demonstrates that building carbon emissions are more closely associated with population distribution than with GDP at the grid scale. While economically productive areas such as central business districts show high emissions coupled with high output, many peripheral zones exhibit relatively high emissions with moderate or low economic returns. This mismatch suggests that improving carbon efficiency requires differentiated strategies: efficiency-oriented measures in high-output cores, demand-side management in dense residential areas, and structural optimization in expanding peripheral districts.

(4) Beyond emissions accounting, the study highlights the future material recovery potential embedded in Guangzhou's building stock. The projected peak in demolition-related material flows during the 2030s reflects the synchronized aging of buildings constructed during the city's rapid expansion phase. This finding emphasizes that urban carbon mitigation and circular economy strategies should be jointly designed, linking building renewal, material recycling, and emission reduction in a coordinated manner.

(5) Despite uncertainties arising from data availability and the use of prototype-based parameters, the proposed framework demonstrates strong applicability for large-scale urban analysis. As more detailed building and energy data become accessible, the accuracy and predictive capacity of this approach can be further improved. More importantly, the methodology is transferable to other cities, providing a scalable tool for comparing urban building carbon trajectories and supporting evidence-based low-carbon planning.

Overall, this study shows that high-resolution, life-cycle-oriented mapping can bridge the gap between building-level assessments and urban-scale policy making. By explicitly linking carbon emissions to building characteristics, spatial structure, and socio-economic drivers, the framework offers actionable insights for cities seeking to balance continued development with long-term carbon reduction goals.

CRediT authorship contribution statement

Tong Sun: Writing – review & editing, Writing – original draft, Visualization, Methodology, Data curation, Conceptualization. **Canjie Liu:** Writing – review & editing, Data curation. **Francesco Pittau:** Writing – review & editing, Project administration. **Lingling Wu:** Writing – review & editing. **Yabo Zhao:** Writing – review & editing, Funding acquisition, Conceptualization.

Declaration of competing interest

The authors declare that they have no known competing financial interests or personal relationships that could have appeared to influence the work reported in this paper.

Acknowledgments

This work was supported by National Natural Science Foundation of China (Grant No 42101186, 42571265), Natural Science Foundation of Guangdong Province (Grant No 2024A1515011291), China's Ministry of Education project of Humanities and Social Science Research (23YJAZH028), Philosophy and Social Science Planning Project of Guangdong Province (GD26CYJ59). Our deepest gratitude goes to the anonymous reviewers and editors for their careful work and thoughtful suggestions that have helped improve this paper substantially.

Supplementary materials

Supplementary material associated with this article can be found, in the online version, at doi:10.1016/j.scs.2026.107641.

Data availability

Data will be made available on request.

References

Abhijna, M., Krishna Rao, K., & Perumal, V. (2025). How new metro lines shape a sustainable future: A before-after study of travel behavior, perceptions, and emissions in Mumbai Metropolitan Region, India. *Sustainable Cities and Society, 127*, Article 106431. https://doi.org/10.1016/j.scs.2025.106431

Al-Qubati, A., Zhang, L., & Forkel, M. (2024). Urban and peri-urban agriculture under climate change: A review on carbon emissions and sequestration. *Sustainable Cities and Society, 115*, Article 105830. https://doi.org/10.1016/j.scs.2024.105830

Anderson, J.R., Hardy, E.E., Roach, J.T., & Witmer, R.E. (1976). A land use and land cover classification system for use with remote sensor data. U.S. Geological Survey Professional Paper 964, iii, 28-p. https://doi.org/10.3133/pp964.

Bampoulas, A., Pallonetto, F., Mangina, E., & Finn, D. (2023). A Bayesian deep-learning framework for assessing the energy flexibility of residential buildings with multicomponent energy systems. *Applied Energy, 348*, Article 121576. https://doi.org/10.1016/j.apenergy.2023.121576

Cai, M., Shi, Y., Ren, C., Yoshida, T., Yamagata, Y., Ding, C., & Zhou, N. (2021). The need for urban form data in spatial modeling of urban carbon emissions in China: A critical review. *Journal of Cleaner Production, 319*, Article 128792. https://doi.org/10.1016/j.jclepro.2021.128792

Cai, W., Pan, T., You, K., Yu, Y., & Li, Y. (2025). Mitigating or pushing? unravelling the dual impact of lifetime on the CO2 emissions from China's urban residential building sector. *Building and Environment, 281*, Article 113236. https://doi.org/10.1016/j.buildenv.2025.113236

Cao, Z., Shen, L., Zhong, S., Liu, L., Kong, H., & Sun, Y. (2018). A probabilistic dynamic material flow analysis model for chinese urban housing stock. *Journal of Industrial Ecology, 22*, 377–391. https://doi.org/10.1111/jiec.12579

Cao, Z., Liu, G., Duan, H., Xi, F., Liu, G., & Yang, W. (2019). Unravelling the mystery of Chinese building lifetime: A calibration and verification based on dynamic material flow analysis. *Applied Energy, 238*, 442–452. https://doi.org/10.1016/j.apenergy.2019.01.106

Carnieletto, L., Ferrando, M., Teso, L., Sun, K., Zhang, W., Causone, F., Romagnoni, P., Zarrella, A., & Hong, T. (2021). Italian prototype building models for urban scale building performance simulation. *Building and Environment, 192*, Article 107590. https://doi.org/10.1016/j.buildenv.2021.107590

Cavalliere, C., Habert, G., Dell'Osso, G., & Hollberg, A. (2019). Continuous BIM-based assessment of embodied environmental impacts throughout the design process. *Journal of Cleaner Production, 211*, 941–952. https://doi.org/10.1016/j.jclepro.2018.11.247

Chang, Y., Huang, Z., Ries, R., & Masanet, E. (2016). The embodied air pollutant emissions and water footprints of buildings in China: A quantification using disaggregated input–output life cycle inventory model. *Journal of Cleaner Production, 113*, 274–284. https://doi.org/10.1016/j.jclepro.2015.11.014

Chastas, P., Theodosiou, T., Kontoleon, K., & Bikas, D. (2018). Normalising and assessing carbon emissions in the building sector: A review on the embodied CO2 emissions of residential buildings. *Building and Environment, 130*, 212–226. https://doi.org/10.1016/j.buildenv.2017.12.032

Christoforatos, G., Pickering, K., Gauss, C., Roy, K., & Beg, M. (2025). Integrating occupancy density into the environmental assessment of residential buildings: Towards embodied impact reduction at both building and urban level. *Building and Environment, 285*, Article 113559. https://doi.org/10.1016/j.buildenv.2025.113559. Part B.

Cook-Patton, S., Leavitt, S., Gibbs, D., Harris, N., Lister, K., Anderson-Teixeira, K., Briggs, R., Chazdon, R., Crowther, T., Ellis, P., Griscom, H., Herrmann, V., Holl, K., Houghton, R., Larrosa, C., Lomax, G., Lucas, R., Madsen, P., Malhi, Y., Paquette, A., Parker, J., Paul, K., Routh, D., Roxburgh, S., Saatchi, S., van den Hoogen, J., Walker, W., Wheeler, C., Wood, S., Xu, L., & Griscom, B. (2020). Mapping carbon accumulation potential from global natural forest regrowth. *Nature, 585*, 545–550. https://doi.org/10.1038/s41586-020-2686-x

Cui, G., Cheng, X., Sun, Y., Gao, C., Duan, Z., & Ruan, T. (2026). High-resolution spatiotemporal dynamic simulation and driving force analysis of carbon emissions in coastal cities: The case of Ningbo City. *Sustainable Cities and Society, 138*, Article 107195. https://doi.org/10.1016/j.scs.2026.107195

Deng, K. (2020). Research on energy use intensity index of office buildings in hot summer and warm winter zone. *M.S. Thesis*. Chongqing, China: Chongqing University (In Chinese) https://doi.org/10.27670/d.cnki.gcqdu.2020.003683.

Dezhi, L., Peng, C., Xin, S., & Ping, C. (2015). In *The Establishment of a Life-cycle Carbon Emission Factor Database for Buildings in China: Presented at the 2015 AASRI International Conference on Circuits and Systems (CAS 2015)*. https://doi.org/10.2991/cas-15.2015.40

Ding, H., Liu, H., & Wang, L. (2009). Preliminary analysis of the energy consumption statistics in civil buildings. *Heating, Ventilation, and Air Conditioning, 39*, 1–3.

Felicioni, L., Gaspari, J., Veselka, J., & Malík, Z. (2023). A comparative cradle-to-grave life cycle approach for addressing construction design choices: An applicative case study for a residential tower in Aalborg, Denmark. *Energy Buildings, 298*, Article 113557. https://doi.org/10.1016/j.enbuild.2023.113557

Fivet, C., De Wolf, C., Menny, T., Vanbutsele, S., & Stephan, A. (2024). Multiscale spatiotemporal characterisation of embodied environmental performance of building structures in Geneva from 1850 to 2018. *Cleaner Environmental Systems, 13*, Article 100194. https://doi.org/10.1016/j.cesys.2024.100194

Gao, J., Liu, H., Tong, Y., & Lou, M. (2024). Hybrid method of mapping urban residential carbon emissions with high-spatial resolution: A case study of Suzhou. *Environment and Planning B: Urban Analytics and City Science, 51*(1), 75–88. https://doi.org/10.1177/23998083231167167

Gauch, H., Dunant, C., Hawkins, W., & Serrenho, A. C. (2023). What really matters in multi-storey building design? A simultaneous sensitivity study of embodied carbon, construction cost, and operational energy. *Applied Energy, 333*, Article 120585. https://doi.org/10.1016/j.apenergy.2022.120585

Geng, J., Wang, J., Huang, J., Zhou, D., Bai, J., Wang, J., Zhang, H., Duan, H., & Zhang, W. (2022). Quantification of the carbon emission of urban residential buildings: The case of the greater bay area cities in China. *Environmental Impact Assessment Review, 95*, Article 106775. https://doi.org/10.1016/j.eiar.2022.106775

Gong, P., Chen, B., Li, X., Liu, H., Wang, J., Bai, Y., Chen, J., Chen, X., Fang, L., Feng, S., Feng, Y., Gong, Y., Gu, H., Huang, H., Huang, X., Jiao, H., Kang, Y., Lei, G., Li, A., Li, X., Li, X., Li, Y., Li, Z., Li, Z., Liu, C., Liu, C., Liu, M., Liu, S., Mao, W., Miao, C., Ni, H., Pan, Q., Qi, S., Ren, Z., Shan, Z., Shen, S., Shi, M., Song, Y., Su, M., Suen, H. P., Sun, B., Sun, F., Sun, J., Sun, L., Sun, W., Tian, T., Tong, X., Tseng, Y., Tu, Y., Wang, H., Wang, L., Wang, X., Wang, Z., Wu, T., Xie, Y., Yang, J., Yang, J., Yuan, M., Yue, W., Zeng, H., Zhang, K., Zhang, N., Zhang, T., Zhang, Y., Zhao, F., Zheng, Y., Zhou, Q., Clinton, N., Zhu, Z., & Xu, B. (2020). Mapping essential urban land use categories in China (EULUC-China). *Science Bulletin, 65*, 182–187. https://doi.org/10.1016/j.scib.2019.12.007

Harris, N., Gibbs, D., Baccini, A., Birdsey, R., De Bruin, S., Farina, M., Fatoyinbo, L., Hansen, M., Herold, M., Houghton, R., Potapov, P., Suarez, D., Roman-Cuesta, R., Saatchi, S., Slay, C., Turubanova, S., & Tyukavina, A. (2021). Global maps of twenty-first century forest carbon fluxes. *Nature Climate, 11*, 234–240. https://doi.org/10.1038/s41558-020-00976-6

Heeren, N., & Fishman, T. (2019). A database seed for a community-driven material intensity research platform. *Scientific Data, 6*, 23. https://doi.org/10.1038/s41597-019-0021-x

Huang, B., Zhao, F., Fishman, T., Chen, W., Heeren, N., & Hertwich, E. (2018). Building material use and associated environmental impacts in China 2000–2015. *Environmental Science & Technology, 52*, 14006–14014. https://doi.org/10.1021/acs.est.8b04104

Huo, T., Li, X., Cai, W., Zuo, J., Jia, F., & Wei, H. (2020). Exploring the impact of urbanization on urban building carbon emissions in China: Evidence from a provincial panel data model. *Sustainable Cities and Society, 56*, Article 102068. https://doi.org/10.1016/j.scs.2020.102068

Hussien, A., Abdeen Saleem, A., Mushtaha, E., Jannat, N., Al-Shammaa, A., Bin Ali, S., Assi, S., Al-Jumeily, D., Bin Ali, S., Assi, S., & Al-Jumeily, D. (2023). A statistical analysis of life cycle assessment for buildings and buildings' refurbishment research. *Ain Shams Engineering Journal, 14*, Article 102143. https://doi.org/10.1016/j.asej.2023.102143

Ito, K., Kang, Y., Zhang, Y., Zhang, F., & Biljecki, F. (2024). Understanding urban perception with visual data: A systematic review. *Cities (London, England), 152*, Article 105169. https://doi.org/10.1016/j.cities.2024.105169

Jungclaus, M., Grant, N., Torres, M., Arehart, J., & Srubar, W. (2024). Embodied carbon benchmarks of single-family residential buildings in the United States, Sustain. *Cities and Society,, 117*, Article 105975. https://doi.org/10.1016/j.scs.2024.105975

Lin, X., Zhu, H., Lin, P., Lin, C., He, H., He, Y., & Chen, Z. (2021). The analysis of survey on road freight transportation in Guangdong Province, China. *Transport Reviews, 43*, 22–27. https://doi.org/10.20164/j.cnki.cn11-1197/u.2021.04.005. Chinese.

Liu, J., Huang, Z., & Wang, X. (2020). Economic and environmental assessment of carbon emissions from demolition waste based on LCA and LCC. *Sustainability, 12*, 6683. https://doi.org/10.3390/su12166683

Liu, T., Zhao, R., Xie, Z., Xiao, L., Chen, A., Feng, W., You, Z., Feng, M., & Li, R. (2023). Carbon emissions from accumulated stock of building materials in China. *Building and Environment, 240*, Article 110451. https://doi.org/10.1016/j.buildenv.2023.110451

Luo, Z., Yang, L., & Liu, J. (2016). Embodied carbon emissions of office building: A case study of China's 78 office buildings. *Building and Environment, 95*, 365–371. https://doi.org/10.1016/j.buildenv.2015.09.018

Luo, Z. (2016). Study on calculation method of building life cycle CO2 emission and emission reduction strategies. *Ph.D. Thesis*. Xi'an, China: Xi'an University of Architecture and Technology (In Chinese).

Ma, Y., Deng, W., Hong, Y., Zhang, H., Ye, Y., Chen, S., & Xu, D. (2025). The advantages and challenges of integrating archetypal building modelling for urban building energy models: A systematic review. *Energy Buildings, 345*, Article 116066. https://doi.org/10.1016/j.enbuild.2025.116066

Malekzadeh, M., Smith, L., Reuschke, D., Farber, S., & Long, J. (2025). Urban mobility and carbon emissions: Decoding the influence of sociodemographic factors, trip-level built environment, and travel behaviour of workers in three UK cities. *Cities (London, England), 167*, Article 106321. https://doi.org/10.1016/j.cities.2025.106321

Mao, R., Bao, Y., Huang, Z., Liu, Q., & Liu, G. (2020). High-resolution mapping of the urban built environment stocks in Beijing. *Environmental Science & Technology, 54*, 5345–5355. https://doi.org/10.1021/acs.est.9b07229

Nayak, B., Sansaniwal, S., Mathur, J., Chandra, T., Garg, V., & Gupta, R. (2023). A review of residential building archetypes and their applications to study building energy consumption. *Architectural Science Review, 66*, 187–200. https://doi.org/10.1080/00038628.2023.2193167

Ng, S., Wong, J., Skitmore, S., & Veronika, A. (2012). Carbon dioxide reduction in the building life cycle: A critical review. *Proceedings of the Institution of Civil Engineers-Engineering Sustainability, 165*, 281–292. https://doi.org/10.1680/ensu.11.00005

Oregi, X., Hermoso, N., Prieto, I., Izkara, J., Mabe, L., & Sismanidis, P. (2018). Automatised and georeferenced energy assessment of an Antwerp district based on cadastral data. *Energy Buildings, 173*, 176–194. https://doi.org/10.1016/j.enbuild.2018.05.018

Pei, W., Biljecki, F., & Stouffs, R. (2024). Techniques and tools for integrating building material stock analysis and life cycle assessment at the urban scale: A systematic literature review. *Building and Environment, 262*, Article 111741. https://doi.org/10.1016/j.buildenv.2024.111741

Pereira, P., & Ramos, N. (2018). Detection of occupant actions in buildings through change point analysis of in-situ measurements. *Energy Buildings, 173*, 365–377. https://doi.org/10.1016/j.enbuild.2018.05.050

Petrova-Antonova, D., Murgante, B., Malinov, S., Nikolova, S., & Ilieva, S. (2025). Walkability analysis of Sofia's neighborhoods powered by 15-minute city concept. *Cities (London, England), 165*, Article 106171. https://doi.org/10.1016/j.cities.2025.106171

Pu, X., Yao, J., & Zheng, R. (2022). Forecast of energy consumption and carbon emissions in China's building sector to 2060. *Energies, 15*, 4950. https://doi.org/10.3390/en15144950

Roncero-Tarazona, M., Ribó-Pérez, D., Rodolfo-Martínez, L., Gil-Chong, P., Montagud-Montalvá, C., & Gómez-Navarro, T. (2025). Scale matters: A 3 scope urban carbon footprint accounting at the neighborhood level, sustain. *Sustainable Cities, 130*, Article 106429. https://doi.org/10.1016/j.scs.2025.106429

Sim, J., & Sim, J. (2017). The atmospheric environmental impact of a Korean traditional building's life cycle, along with carbon footprint analysis. *Sustainable Cities and Society, 28*, 172–186. https://doi.org/10.1016/j.scs.2016.09.008

United Nations Environment Programme. (2020). 2020 Global Status Report for Buildings and Construction: Towards a Zero-emission, Efficient and Resilient Buildings and Construction Sector. Nairobi: United Nations Environment Programme. https://globalabc.org/resources/publications/2020-global-status-report-buildings-and-construction. Accessed 22 January 2025.

Wang, S., Liu, X., Zhou, C., Hu, J., & Ou, J. (2017). Examining the impacts of socioeconomic factors, urban form, and transportation networks on CO2 emissions in China's megacities. *Applied Energy, 185*, 189–200. https://doi.org/10.1016/j.apenergy.2016.10.052

Wang, G., Hu, Q., He, L., Guo, J., Huang, J., & Zhong, L. (2024). The estimation of building carbon emission using nighttime light images: A comparative study at various spatial scales. *Sustainable Cities and Society, 101*, Article 105066. https://doi.org/10.1016/j.scs.2023.105066

Xu, S., Wang, S., Li, G., Zhou, H., Meng, C., Qin, Y., & He, B. (2024). Performance-based design of residential blocks for the co-benefits of building energy efficiency and outdoor thermal comfort improvement. *Building and Environment, 264*, Article 111926. https://doi.org/10.1016/j.buildenv.2024.111926

Yang, D., Guo, J., Sun, L., Shi, F., Liu, J., & Tanikawa, H. (2020). Urban buildings material intensity in China from 1949 to 2015. *Resources, Conservation and Recycling, 159*, Article 104824. https://doi.org/10.1016/j.resconrec.2020.104824

Yang, F., Yang, D., Zhang, Y., Guo, R., Li, J., & Wang, H. (2024). Evaluating the multi-seasonal impacts of urban blue-green space combination models on cooling and carbon-saving capacities. *Building and Environment, 266*, Article 112045. https://doi.org/10.1016/j.buildenv.2024.112045

Yigit, S., Zambrano, J. M., & Baldini, L. (2025). A GIS and bottom-up simulation-based framework to assess the role of zero-emission building standards in achieving low-carbon goals: Insights from a case study for China. In U. Berardi, J. António, & N. Simões (Eds.)*, 744*. *Construction, Energy, Environment and Sustainability. ICCEES 2025. Lecture Notes in Civil Engineering* (pp. 413–422). Singapore: Springer. https://doi.org/10.1007/978-981-95-1826-5_44.

Luo, Z., Cang, Y., Zhang, N., Yang, L., & Liu, J. (2019). A quantitative process-based inventory study on material embodied carbon emissions of residential, office, and commercial buildings in China. *Journal of Thermal Science, 28*, 1236–1251. https://doi.org/10.1007/s11630-019-1165-x

Zhang, Z., & Wang, B. (2016a). Research on the life-cycle CO2 emission of China's construction sector. *Energy Buildings, 112*, 244–255. https://doi.org/10.1016/j.enbuild.2015.12.026

Zhang, X., & Wang, F. (2016b). Assessment of embodied carbon emissions for building construction in China: Comparative case studies using alternative methods. *Energy and Buildings, 130*, 330–340. https://doi.org/10.1016/j.enbuild.2016.08.080

Zhang, Y., Hu, S., Guo, F., Mastrucci, A., Zhang, S., Yang, Z., & Yan, D. (2022). Assessing the potential of decarbonizing China's building construction by 2060 and synergy with industry sector. *Journal of Cleaner Production, 359*, Article 132086. https://doi.org/10.1016/j.jclepro.2022.132086

Zhang, L., Zhou, J., Xi, W., & Wang, J. (2025). Spatio-temporal pattern evolution of energy consumption carbon emissions at the city and county levels based on the population-kNDVI correction of nighttime light from 2000 to 2020. *Sustainable Cities and Society, 130*, Article 106655. https://doi.org/10.1016/j.scs.2025.106655

Zhou, Y., Shan, Y., Liu, G., & Guan, D. (2018). Emissions and low-carbon development in Guangdong-Hong Kong-Macao Greater Bay Area cities and their surroundings. *Applied Energy, 228*, 1683–1692. https://doi.org/10.1016/j.apenergy.2018.07.038

Zhou, X. (2022). Analysis and research on electricity consumption monitoring data of public buildings in pearl river delta region. *Construction Science and Technology, 18*, 79–82. https://doi.org/10.16116/j.cnki.jskj.2022.18.021

Zhu, C., Li, X., Zhu, W., & Gong, W. (2022). Embodied carbon emissions and mitigation potential in China's building sector: An outlook to 2060. *Energy Policy, 170*, Article 113222. https://doi.org/10.1016/j.enpol.2022.113222